

# The ROSAT deep survey <sup>\*</sup>

## V. X-ray Sources and Optical Identifications in the Marano Field

G.Zamorani<sup>1,2</sup>, M.Mignoli<sup>1</sup>, G. Hasinger<sup>3</sup>, R.Burg<sup>4</sup>, R.Giacconi<sup>5</sup>, M.Schmidt<sup>6</sup>, J.Trümper<sup>7</sup>, P.Ciliegi<sup>1</sup>, C.Gruppioni<sup>1</sup>, and B.Marano<sup>1,8</sup>

<sup>1</sup> Osservatorio Astronomico di Bologna, Via Ranzani 1, 40127 Bologna, Italy

<sup>2</sup> Istituto di Radioastronomia del CNR, via Gobetti 101, 40129 Bologna, Italy

<sup>3</sup> Astrophysikalisches Institut Potsdam, An der Sternwarte 16, D-14482 Potsdam, Germany

<sup>4</sup> Johns Hopkins University, Baltimore, MD 21218, USA

<sup>5</sup> European Southern Observatory, Karl-Schwarzschild-Str. 1, D-85748 Garching bei München, Germany

<sup>6</sup> California Institute of Technology, Pasadena, CA 91125, USA

<sup>7</sup> Max-Planck-Institut für extraterrestrische Physik, Karl-Schwarzschild-Str. 2, D-85748 Garching bei München, Germany

<sup>8</sup> Dipartimento di Astronomia, Università di Bologna, Via Ranzani 1, 40127 Bologna, Italy

Received 21 January 1999 / Accepted 26 March 1999

**Abstract.** We present the X-ray data and the optical identifications for a deep ROSAT PSPC observation in the “Marano field”. In the inner region of the ROSAT field (15′ radius) we detected 50 X-ray sources with  $S_x \geq 3.7 \times 10^{-15} \text{ erg cm}^{-2} \text{ s}^{-1}$ . When corrected for the different sensitivity over the field, the estimated observed surface density at  $S_x \geq 4 \times 10^{-15} \text{ erg cm}^{-2} \text{ s}^{-1}$  is  $272 \pm 40$  sources/sq.deg. Four X-ray sources, corresponding to 8% of the total sample, have been detected in radio images with a flux limit of about 0.2 mJy.

Careful statistical analysis of multi-colour CCD data in the error boxes of the 50 X-ray sources has led to the identification of 42 sources, corresponding to 84% of the X-ray sample. These 42 reliable identifications are 33 AGNs (including two radio galaxies and one BL Lac candidate; 79% of the identified sources), 2 galaxies, 3 groups or clusters of galaxies and 4 stars. If we divide our sample into two equally populated sub-samples as a function of flux, at  $S_x = 6.5 \times 10^{-15} \text{ erg cm}^{-2} \text{ s}^{-1}$ , we find that the percentage of identifications remains approximately constant (88% and 80% in the high and low flux sub-samples, respectively). AGNs are the dominant class of objects in both sub-samples (90% of the optical identifications in the high flux sub-sample and 65% in the low flux sub-sample), while the few identifications with clusters and galaxies are all in the low flux sub-sample.

We also show that it is likely that a few of the 8 unidentified sources are such because the derived X-ray positions may be offset with respect to the real ones due to confu-

sion effects. The unidentified sources have a large ratio of X-ray to optical fluxes and most of them have harder than average X-ray spectra. Since most of the identified objects with these characteristics in our field and in the Lockman field are AGNs, we conclude that also most of these sources are likely to be AGNs.

Finally, comparing the optically and X-ray selected samples of AGNs in this field, we estimate that the “efficiency” of AGN selection with X-ray exposures reaching about  $4 \times 10^{-15} \text{ erg cm}^{-2} \text{ s}^{-1}$  is  $\sim 65\%$  and  $\sim 20\%$  in the magnitude ranges  $m_B < 22.5$  and  $22.5 < m_B < 23.5$ , respectively. On the other hand, a not negligible fraction of the X-ray selected AGNs would have not been easily selected as AGN candidates on the basis of purely optical criteria, either because of colours similar to those of normal stars or because of morphological classification not consistent with that of point-like sources.

**Key words:** surveys - cosmology: diffuse radiations - X-rays: galaxies - galaxies:active - quasars: emission lines - galaxies: Seyfert

Send offprint requests to: G. Zamorani (zamorani@bo.astro.it)

<sup>\*</sup> based on observations collected at the European Southern Observatory, La Silla, Chile.

### 1. Introduction

Complete or, at least, statistically well defined samples of optical identifications of faint X-ray sources, are important for a number of scientific goals. For example, combined optical and X-ray data allow to obtain information about the luminosity functions of various types of X-ray sources as well as their evolution with redshift.

In turn, these informations can be used to further constrain models for the production of the X-ray background, discovered more than thirty years ago (Giacconi et al. 1962). There is a general consensus that the majority of the optically identified X-ray sources, at least for fluxes  $S_{0.5-2\text{keV}} \geq 5 \times 10^{-15} \text{ erg cm}^{-2} \text{ s}^{-1}$ , are active galactic nuclei (AGNs), i.e. quasars and Seyfert galaxies with broad emission lines (Shanks et al. 1991, Georgantopoulos et al. 1996, McHardy et al. 1998, Hasinger et al. 1998 (Paper I) and Schmidt et al. 1998 (Paper II)).

In the first two papers of this series we have presented the X-ray and optical data for a complete catalogue of 50 X-ray sources with PSPC fluxes (0.5-2 keV) above  $5.5 \times 10^{-15} \text{ erg cm}^{-2} \text{ s}^{-1}$  in the Lockman Field. Optical and X-ray results at a much fainter flux limit in this field, which has been observed with the deepest ROSAT PSPC and HRI observations, will be presented elsewhere.

In this paper we present and discuss the X-ray data (Section 2) and the optical data (Section 3) for 50 sources detected with the PSPC at a flux limit  $S_x \geq 3.7 \times 10^{-15} \text{ erg cm}^{-2} \text{ s}^{-1}$  in the Marano Field. A discussion of the main results (percentages of identifications with different classes of objects, hardness ratio as a function of X-ray flux, comparison between X-ray and optically selected AGNs) is given in Section 4. Throughout the paper we use  $H_0 = 50 \text{ km s}^{-1} \text{ Mpc}^{-1}$  and  $q_0 = 0.5$ .

## 2. The X-ray Data

### 2.1. The sample

The ROSAT–PSPC pointed observations of the Marano field, centered at RA =  $03^{\text{h}}15^{\text{m}}09^{\text{s}}$ , DEC =  $-55^{\circ}13'57''$  (epoch 2000.0), have been carried out in the time interval December 1992 – July 1993, for a total of 56 ksec of observing time. The observations were performed in the “wobble mode”.

The X-ray analysis (e.g. source detection, position and flux determination of the detected sources, determination of sensitivity as a function of distance from the center, etc.) has been done applying a maximum likelihood method. For details about the various steps in this analysis we refer the reader to Hasinger et al. (1993 and 1998). Although detection of the sources has been run in various ROSAT bands, we report here results only for the hard band (0.5–2 keV), which has been shown (Hasinger et al. 1993) to be the most efficient for point source detection.

Table 1 contains the X-ray data for the complete sample of sources in a circular area with radius of  $15'$ . Within this area we detected 50 sources with a maximum likelihood value  $ML \geq 9.8$ . With this adopted threshold in ML we expect less than one spurious source over the entire area. The first column gives an identification code for the X-ray sources: the first number identifies the sources in our working lists, while the second one (from 1 to 50) represents the source rank in order of decreasing X-ray

flux. Columns 2 to 5 give the  $\alpha$  (2000) and  $\delta$  (2000) positions, with the one sigma error on each coordinate (in arcsec) derived from the maximum likelihood fitting, and the off-axis distance from the center of the X-ray field (in arcmin). The next three columns give the maximum likelihood value in the hard band, the net counts and the corresponding 0.5 – 2.0 keV flux and error. The flux has been computed assuming the same intrinsic spectrum for all the sources, i.e. a power law spectrum with a slope  $\alpha = 1.0$ , with no intrinsic absorption and a galactic absorption corresponding to  $N_H = 2.5 \times 10^{20}$ . These assumed parameters correspond to the conversion factor  $1 \text{ ct/s} = 2.26 \times 10^{-12} \text{ erg cm}^{-2} \text{ s}^{-1}$  at the center of the field. The last column gives the hardness ratio with its statistical error.

Since most of the detected X-ray sources are too faint to obtain a full resolution spectrum, we have characterized their spectra using the hardness ratio technique. The hardness ratio is defined as  $HR=(H-S)/(H+S)$ , where S and H are the net counts in the PSPC energy channels 11–41 and 52–201, respectively, corresponding approximately to the energy ranges 0.1–0.4 and 0.5–2.0 keV. The source counts in each band have been obtained summing all the counts from a circle centered at the source position. The radius of the extraction circle was  $60''$ . However, when the extraction circles of two sources overlapped, this radius was reduced to  $30''$  in order to avoid contamination from the nearby source. The resulting net counts for the instrumental radial vignetting and for the energy dependence of the ROSAT/PSPC Point Spread Function (Hasinger et al. 1994). The background counts were estimated in a circular area near the source position, after excluding the contribution from near-by sources. Five sources, corresponding to 10% of the total sample, have a formal hardness ratio equal to or greater 1.00 (i.e. zero or negative net counts detected in the soft band). Four of them are at the faint flux limit of the entire sample.

To eliminate a possible systematic error of a few arcsec in the X-ray positions, we have cross-correlated the positions of the 50 X-ray sources within  $15'$  from the center with those of 29 previously known optically selected AGNs with  $m_B \leq 22.5$  in the same area (Zitelli et al. 1992; Mignoli et al. in preparation). We have found 19 positional coincidences, with distances smaller than  $12''$  between X-ray and optical positions, while less than 0.3 random coincidences are expected on a statistical basis. The average offset between X-ray and optical positions is about  $4''$  in right ascension and less than  $1''$  in declination, with no additional trend as a function of position in the field. The one sigma uncertainty for the offset in each coordinate is of the order of  $0.9''$ . We have therefore applied this average offset to all the original X-ray positions and corrected the ML positional errors by adding in quadrature the uncertainty on the offset. Both the positions and the positional errors given in Table 1 are the “corrected” values.

Figure 1 shows a gray scale representation of the hard ROSAT image. The image has been slightly smoothed

**Table 1.** The X-ray Data

| #       | RA (2000) | DEC (2000) | Err<br>[arcsec] | Off-axis<br>[arcmin] | ML    | Net Counts | $S_x$<br>[ $\times 10^{-14}$ cgs] | HR               |
|---------|-----------|------------|-----------------|----------------------|-------|------------|-----------------------------------|------------------|
| X013-01 | 3 13 47.1 | -55 11 48  | 1.6             | 12.1                 | 448.2 | 210.1      | $5.00 \pm 0.42$                   | $-0.03 \pm 0.06$ |
| X012-02 | 3 13 29.2 | -55 10 20  | 2.7             | 14.8                 | 203.3 | 155.7      | $3.82 \pm 0.37$                   | $0.41 \pm 0.12$  |
| X046-03 | 3 14 32.4 | -55 14 43  | 1.6             | 5.5                  | 303.1 | 130.1      | $2.99 \pm 0.32$                   | $0.20 \pm 0.10$  |
| X036-04 | 3 16 50.3 | -55 11 10  | 2.4             | 14.5                 | 175.4 | 118.9      | $2.91 \pm 0.30$                   | $-0.10 \pm 0.08$ |
| X021-05 | 3 14 56.4 | -55 20 08  | 1.8             | 6.7                  | 190.4 | 102.3      | $2.36 \pm 0.25$                   | $0.88 \pm 0.20$  |
| X025-06 | 3 15 49.5 | -55 18 11  | 1.8             | 7.1                  | 184.7 | 99.8       | $2.31 \pm 0.30$                   | $0.28 \pm 0.13$  |
| X027-07 | 3 16 05.5 | -55 15 44  | 2.2             | 8.1                  | 124.6 | 71.8       | $1.66 \pm 0.28$                   | $-0.21 \pm 0.10$ |
| X041-08 | 3 15 28.7 | -55 10 32  | 2.6             | 4.1                  | 99.7  | 62.0       | $1.42 \pm 0.25$                   | $0.58 \pm 0.15$  |
| X240-09 | 3 16 38.2 | -55 06 41  | 3.9             | 14.4                 | 56.1  | 50.9       | $1.25 \pm 0.24$                   | $0.45 \pm 0.25$  |
| X033-10 | 3 15 58.3 | -55 26 40  | 4.2             | 14.6                 | 46.7  | 50.9       | $1.25 \pm 0.23$                   | $-0.48 \pm 0.11$ |
| X042-11 | 3 15 40.4 | -55 12 25  | 2.3             | 4.5                  | 77.1  | 52.4       | $1.20 \pm 0.18$                   | $0.32 \pm 0.32$  |
| X043-12 | 3 15 09.8 | -55 13 18  | 2.3             | 0.5                  | 88.2  | 48.5       | $1.10 \pm 0.25$                   | $0.37 \pm 0.32$  |
| X023-13 | 3 15 25.2 | -55 18 28  | 2.7             | 5.2                  | 59.1  | 43.5       | $1.00 \pm 0.17$                   | $-0.27 \pm 0.19$ |
| X108-14 | 3 15 37.9 | -55 01 42  | 4.4             | 12.7                 | 30.8  | 41.0       | $0.98 \pm 0.20$                   | $0.63 \pm 0.62$  |
| X030-15 | 3 16 26.1 | -55 23 00  | 4.3             | 14.2                 | 28.3  | 39.6       | $0.97 \pm 0.18$                   | $0.03 \pm 0.20$  |
| X304-16 | 3 15 11.4 | -55 09 30  | 3.1             | 4.3                  | 56.5  | 40.8       | $0.94 \pm 0.18$                   | $0.08 \pm 0.27$  |
| X019-17 | 3 14 21.8 | -55 23 55  | 3.6             | 12.3                 | 43.0  | 38.8       | $0.93 \pm 0.27$                   | $0.24 \pm 0.31$  |
| X029-18 | 3 16 29.9 | -55 19 06  | 3.8             | 12.5                 | 30.1  | 37.0       | $0.89 \pm 0.17$                   | $0.14 \pm 0.30$  |
| X039-19 | 3 15 52.9 | -55 08 20  | 3.2             | 8.1                  | 47.5  | 38.0       | $0.88 \pm 0.18$                   | 1.00             |
| X001-20 | 3 15 20.7 | -55 02 33  | 3.6             | 11.3                 | 46.4  | 37.4       | $0.88 \pm 0.26$                   | $-0.07 \pm 0.24$ |
| X049-21 | 3 15 06.0 | -55 09 42  | 3.0             | 4.1                  | 49.4  | 35.9       | $0.82 \pm 0.21$                   | $-0.19 \pm 0.20$ |
| X211-22 | 3 13 45.5 | -55 19 25  | 4.4             | 13.4                 | 21.5  | 33.8       | $0.81 \pm 0.19$                   | $-0.08 \pm 0.32$ |
| X404-23 | 3 16 48.9 | -55 12 40  | 9.3             | 14.1                 | 10.2  | 29.7       | $0.73 \pm 0.21$                   | 1.00             |
| X031-24 | 3 15 48.7 | -55 22 50  | 4.4             | 10.6                 | 17.4  | 30.2       | $0.71 \pm 0.18$                   | $-0.21 \pm 0.29$ |
| X050-25 | 3 15 07.6 | -55 04 58  | 3.8             | 8.8                  | 10.0  | 30.1       | $0.70 \pm 0.16$                   | $-0.26 \pm 0.23$ |
| X235-26 | 3 16 31.7 | -55 12 27  | 5.2             | 11.7                 | 14.3  | 26.7       | $0.63 \pm 0.18$                   | $0.21 \pm 0.45$  |
| X045-27 | 3 15 10.7 | -55 15 23  | 3.5             | 1.6                  | 30.8  | 26.9       | $0.61 \pm 0.15$                   | $0.24 \pm 0.33$  |
| X409-28 | 3 14 26.3 | -55 17 41  | 5.2             | 7.4                  | 22.0  | 26.2       | $0.61 \pm 0.14$                   | $0.84 \pm 0.85$  |
| X301-29 | 3 14 36.3 | -55 14 04  | 4.1             | 4.9                  | 20.2  | 26.0       | $0.60 \pm 0.15$                   | $-0.21 \pm 0.27$ |
| X408-30 | 3 14 50.3 | -55 19 39  | 4.1             | 6.6                  | 17.1  | 25.6       | $0.59 \pm 0.16$                   | $0.65 \pm 0.87$  |
| X207-31 | 3 13 50.3 | -55 13 00  | 4.9             | 11.5                 | 16.1  | 24.7       | $0.59 \pm 0.15$                   | $-0.12 \pm 0.42$ |
| X040-32 | 3 15 43.1 | -55 07 46  | 3.5             | 7.6                  | 27.5  | 24.9       | $0.58 \pm 0.14$                   | $0.34 \pm 0.41$  |
| X028-33 | 3 16 21.8 | -55 18 00  | 4.8             | 11.0                 | 16.5  | 23.8       | $0.56 \pm 0.14$                   | $0.24 \pm 0.45$  |
| X250-34 | 3 15 23.3 | -55 04 03  | 4.4             | 9.9                  | 17.4  | 24.0       | $0.56 \pm 0.14$                   | $0.65 \pm 0.31$  |
| X011-35 | 3 13 39.9 | -55 07 21  | 6.1             | 14.4                 | 11.2  | 22.7       | $0.56 \pm 0.15$                   | $0.04 \pm 0.37$  |
| X032-36 | 3 15 38.7 | -55 22 33  | 5.4             | 9.7                  | 13.4  | 23.2       | $0.54 \pm 0.14$                   | $-0.01 \pm 0.43$ |
| X251-37 | 3 15 31.0 | -55 04 43  | 6.0             | 9.5                  | 16.8  | 22.5       | $0.52 \pm 0.14$                   | $0.07 \pm 0.67$  |
| X024-38 | 3 15 34.7 | -55 19 27  | 5.4             | 6.7                  | 12.4  | 22.7       | $0.52 \pm 0.16$                   | $-0.11 \pm 0.23$ |
| X015-39 | 3 13 51.6 | -55 18 33  | 6.9             | 12.2                 | 11.8  | 21.4       | $0.51 \pm 0.14$                   | $-0.43 \pm 0.22$ |
| X236-40 | 3 16 24.0 | -55 11 44  | 4.3             | 10.7                 | 15.9  | 21.3       | $0.50 \pm 0.13$                   | $0.02 \pm 0.32$  |
| X234-41 | 3 16 23.7 | -55 15 17  | 5.3             | 10.6                 | 10.7  | 20.7       | $0.48 \pm 0.15$                   | $-0.15 \pm 0.41$ |
| X306-42 | 3 15 50.1 | -55 09 15  | 4.5             | 7.2                  | 17.0  | 20.1       | $0.47 \pm 0.14$                   | $-0.22 \pm 0.38$ |
| X051-43 | 3 15 01.6 | -55 03 40  | 6.6             | 10.2                 | 11.1  | 19.9       | $0.46 \pm 0.14$                   | $0.93 \pm 1.00$  |
| X407-44 | 3 14 12.4 | -55 25 52  | 7.3             | 14.7                 | 9.8   | 18.2       | $0.45 \pm 0.14$                   | $-0.33 \pm 0.25$ |
| X233-45 | 3 16 18.9 | -55 14 29  | 7.2             | 9.8                  | 9.8   | 19.3       | $0.45 \pm 0.14$                   | $0.26 \pm 0.41$  |
| X109-46 | 3 16 08.1 | -55 17 25  | 4.8             | 9.0                  | 11.9  | 18.3       | $0.43 \pm 0.12$                   | $0.05 \pm 0.30$  |
| X213-47 | 3 14 12.1 | -55 18 24  | 5.4             | 9.5                  | 11.7  | 17.9       | $0.42 \pm 0.14$                   | 1.00             |
| X022-48 | 3 15 03.4 | -55 19 06  | 4.4             | 5.4                  | 12.3  | 18.3       | $0.42 \pm 0.12$                   | 1.00             |
| X215-49 | 3 14 29.6 | -55 16 44  | 5.3             | 6.5                  | 12.3  | 17.7       | $0.41 \pm 0.12$                   | 1.00             |
| X264-50 | 3 14 49.1 | -55 22 24  | 5.2             | 9.2                  | 12.0  | 15.8       | $0.37 \pm 0.14$                   | 1.00             |

**Fig. 1.** Gray scale representation of the hard ROSAT image. The image has been slightly smoothed with a gaussian filter with  $\sigma = 10''$ . All the 50 sources detected within a radius of  $15'$  are labelled.

with a gaussian with  $\sigma = 10''$ . All the sources detected within a radius of  $15'$  are labelled. The figure shows the capability of the maximum likelihood algorithm in retrieving pairs of sources relatively close to each other (see, for example, the two pairs 49–304 and 46–301, for which the distances between the X-ray positions are of the order of 50 arcsec). For distances between two X-ray centroids smaller than  $\sim 40''$ , however, our detection algorithm is unable to separate the two X-ray sources and will find a single source (Hasinger et al. 1993), with a position intermediate between the two true positions. In these cases the resulting X-ray position and its associated error would not be reliable and this would lead to problems in the optical identification process.

In order to estimate how many such cases we may have in our list of sources we have simulated 1000 random samples with the same number of detected sources and with the same radial surface densities of sources as the real sample (i.e. higher density in the inner region of the field and lower density in the outer region). For each sample we have then computed the number of sources which have a nearby companion at a distance smaller than the smallest observed distance in the real sample (i.e.  $48''$ ). Figure 2 shows the normalized histogram of the number of such sources in the 1000 random samples. The figure shows that in only 2% of the cases there is no pair of sources with a distance smaller than 48 arcsec, while in the central 75%

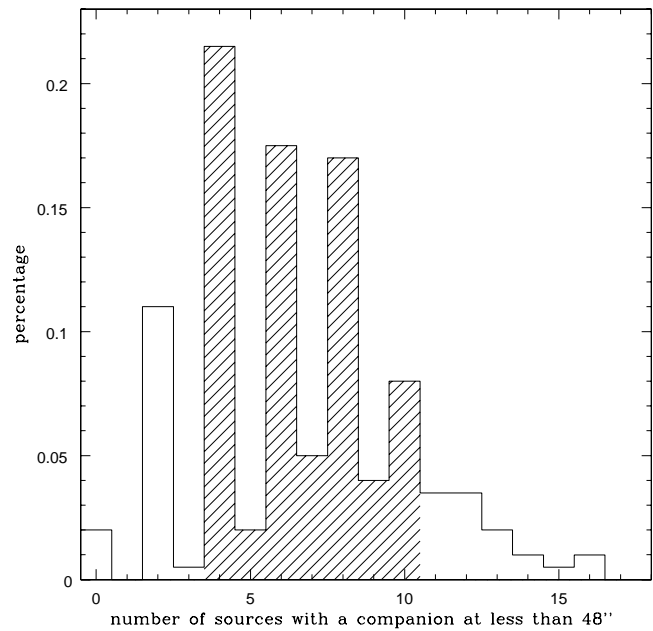


**Fig. 2.** Histogram of the number of sources with a companion at less than  $48''$  in 1000 simulated samples. In 75% of the cases the number of these sources is between 4 and 10 (hatched area).

of the cases (hatched area) the number of such sources ranges from 4 to 10.

Since each pair is counted twice in this histogram, this means that we may expect that in about 2–5 cases a single source in our list may be produced by two different close-by sources, so that its position may be significantly wrong and we may not be able to find any reliable optical counterpart within the error box. Note that this estimate is based on purely geometric considerations; moreover, since in computing the expected number of close-by sources we have adopted the observed surface density of sources, we are not considering in this order of magnitude estimate the cases in which one or both the sources in a close pair are below the detection limit. Results from more detailed simulations, which take into account all the possible effects of source confusion, are discussed in Hasinger et al. (1998).

Figure 3 shows the hard X-ray flux versus the off-axis angle for all the X-ray sources listed in Table 1. Even if we have considered only sources within  $15'$  from the center, the limiting flux is not constant over the adopted field of view. Its increase at distances greater than about  $10'$  is mainly due to the increase of the width of the point spread function with the off-axis angle. The curve drawn in the figure shows our estimated limiting flux as a function of the off-axis angle for the complete sample. When corrected for the different sensitivity over the field, and using only the 48 sources with flux greater than the adopted limiting flux, the estimated observed surface density at

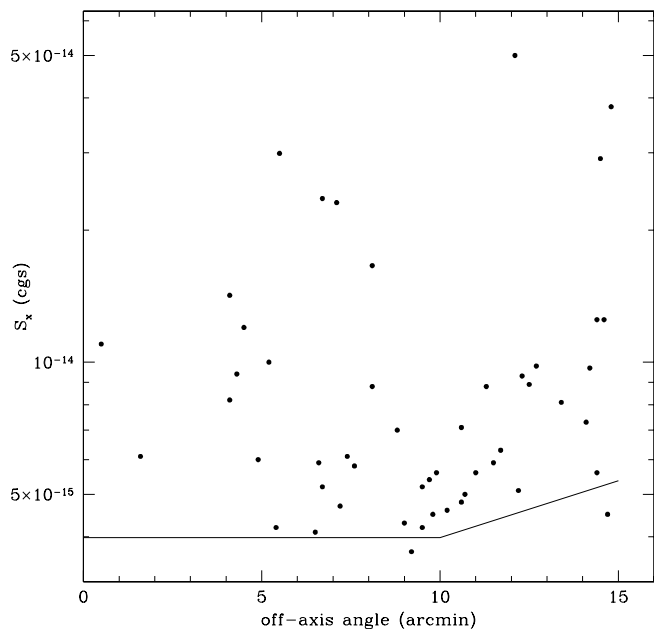


**Fig. 3.** Hard X-ray flux versus the off-axis angle for all the X-ray sources listed in Table 1. The curve shows the limiting flux as a function of off-axis angle which has been used to estimate the “corrected” observed surface density of sources.

$S_x \geq 4 \times 10^{-15} \text{ erg cm}^{-2} \text{ s}^{-1}$  is  $272 \pm 40$  sources/sq.deg. This value is consistent with the surface density (248 sources/sq.deg.) derived by Hasinger et al. (1993) from the composite observed  $\log N - \log S$  relationship using the deeper ROSAT data in the Lockman Hole together with a number of shallower fields.

### 3. The Identification of the X-ray Sources

#### 3.1. The Radio Data

We observed the Marano field at 1.4 and 2.4 GHz with the Australia Telescope Compact Array (ATCA). The radio observations were carried out on 1994 January 4, 5, 6 and 7. Details about the radio observation and data reduction are given in Gruppioni et al. (1997), where catalogs of  $5\sigma_{local}$  radio sources are given. The radio limits are about 0.2 mJy at both frequencies. Cross-correlation of the entire radio and X-ray catalogs has produced four positional coincidences with a maximum difference of  $\sim 10''$  between radio and X-ray positions. All these distances are between 1.1 and 2.4 times the combined X-ray and radio positional error ( $\epsilon$ ). Fifteen more radio – X-ray pairs have distances smaller than  $90''$ , but none has a distance smaller than  $25''$ . For all these pairs the distances between radio and X-ray positions are larger than five times the combined positional error and can therefore be considered random coincidences. From the number of these random pairs we

**Table 2.** The Radio – X-ray Coincidences

| X-ray   |                                  | Radio |               | Distance             |                   |
|---------|----------------------------------|-------|---------------|----------------------|-------------------|
| #       | flux<br>[ $\times 10^{-14}$ cgs] | #     | flux<br>[mJy] | $\Delta$<br>[arcsec] | $\Delta/\epsilon$ |
| X013–01 | 5.00                             | 15    | 158           | 3.8                  | 2.0               |
| X021–05 | 2.36                             | 38    | 1.25          | 2.3                  | 1.1               |
| X409–28 | 0.61                             | 30    | 6.32          | 8.2                  | 1.5               |
| X408–30 | 0.59                             | 35    | 0.41          | 10.3                 | 2.4               |

estimate that the expected number of similarly random pairs within  $10''$  is  $0.20 \pm 0.05$ . If, instead of using a radius of  $10''$ , which can be considered an “a posteriori” choice, we use for each X-ray source a radius corresponding to the 95% error circle, the estimated number of random pairs inside the 95% area becomes 0.40. On this basis we conclude that probably none and at most one of the observed radio – X-ray coincidences is not real. The four radio – X-ray pairs correspond to a percentage of radio detection of  $8 \pm 4\%$  for our X-ray sources at a radio limit of  $\sim 0.2$  mJy. Of the same order ( $10 \pm 5\%$ ) is the percentage of X-ray detections for our sample of radio sources. Both these percentages are in good agreement with what has been found by De Ruiter et al. (1996) from VLA observations in the region of the Lockman Hole. Table 2 lists these four radio – X-ray pairs, where the columns are X-ray number and flux from Table 1, radio number and flux from the 20 cm catalog in Gruppioni et al. 1997, difference in position ( $\Delta$ ) in arcsec and normalized to the combined X-ray and radio error ( $\Delta/\epsilon$ ). Three of these four radio – X-ray pairs have been optically identified (see Section 3.2). For all of them the offset between the radio and the optical position of the suggested identification is less than  $1.8''$ , consistent with the combined radio and optical positional errors.

#### 3.2. The Optical Data

In addition to the ESO 3.6m plates (U, J, F bands) which were already available and have been used in the past to obtain a complete sample of optically selected AGNs with  $m_B \leq 22.0$  (Zitelli et al. 1992), in the years 1992–1994 we have obtained a set of U, B, V, R CCD images at the ESO NTT. The V and R images cover  $\sim 90\%$  of the circle with  $15'$  radius and contain all but one of the X-ray sources within this radius; the U and B images, which have a smaller field of view, cover a smaller fraction of the  $15'$  field, but still contain 45 out of 50 X-ray sources. Details about the observations, data reduction and optical catalogs obtained from these CCD observations will be given elsewhere (Mignoli et al. in preparation; see also Mignoli 1997).

The CCD limiting magnitudes vary from field to field, but typically are of the order of 23.5 in U, 25.0 in B, 24.0 in V and R. The typical surface density of objects at these limits is  $\sim 60,000$  per square degree. Since the

total area covered by the  $2\sigma$  ( $3\sigma$ ) error circles of the 50 X-ray sources corresponds to 5.4 (10.4) sq.arcmin., this implies a total expected number of  $\sim 90$  (175) catalogued objects inside the X-ray error boxes. In Table 3 we report the optical data for all the objects in our optical catalogs within a  $3\sigma$  error box, plus a few interesting objects at slightly larger distance. (We recall that, under the assumption that the distribution function of the positional errors follows a circular normal distribution, the  $1\sigma$ ,  $2\sigma$  and  $3\sigma$  error boxes correspond to radii equal to 1.51, 2.45 and 3.4 times the error in each coordinate, respectively.) The first ten columns in the Table give the X-ray number, the distance in right ascension and declination between the X-ray source and the optical objects (arcsec), the total distance both in arcsec and normalized to the X-ray positional error ( $\varepsilon_x$ ) as defined in Section 2.1, optical B and R magnitudes and U-B, B-V, V-R colours and a morphological classification (p for point-like source, e for extended, p/e or e/p for sources classified differently in the blue and red bands). The morphological classification is reliable only for objects which are more than  $\sim 1.5$  magnitudes brighter than the limiting magnitude (Flynn, Gould and Bahcall 1996). An asterisk in the magnitude columns means that the magnitudes have been measured from the plates and then converted to the Johnson system (see Gruppioni, Mignoli and Zamorani 1999).

The next two columns give the likelihood ratio (LR) computed from the B and R data. These LR values have been computed following the procedure described by Sutherland and Saunders (1992), which, differently from previous formulations, has been shown to be valid also in the case of multiple candidates in the error boxes. For each optical object its likelihood ratio is defined as:

$$LR = \frac{q(m, c) f(x, y)}{n(m, c)} \quad (1)$$

where  $f(x, y)$  is the probability distribution function of the positional errors,  $n(m, c)$  is the surface density of “background” objects with magnitude  $m$  and type  $c$  and  $q(m, c)$  is the probability distribution function in magnitude and type of the optical counterparts. With this definition LR is the ratio between the probability of finding the true optical counterpart with the observed offset  $(x, y)$  from the X-ray position and the observed magnitude and the probability of finding a similar chance background object (see Eq. 1 and related discussion in Sutherland and Saunders 1992). Assuming that the distribution function of the positional errors is gaussian,

$$f(x, y) = \frac{e^{-\frac{(x^2+y^2)}{2\sigma^2}}}{2\pi\sigma^2} \quad (2)$$

where  $x$  and  $y$  are the offsets in right ascension and declination between the optical and X-ray sources and  $\sigma$  is the positional error in each coordinate (see column 4 in Table 1). We considered two different types of optical objects,

i.e. point-like and extended. For each of them the observed  $n(m)$  has been obtained from our own CCD data, while  $q(m)$  has been estimated from the magnitude distribution of the excess of objects in the 50 X-ray error boxes with respect to the expected number of “background” objects.

The last two columns give the redshift and the classification of the objects based on our spectroscopic data. Objects which we consider to be the correct identification are written in bold face in the last column. When the spectroscopic data suggest identification with a group or cluster of galaxies, all the galaxies at the redshift of the cluster are shown in bold face.

Figure 4 shows the finding charts for all the X-ray sources within  $15'$ , ordered by decreasing X-ray flux, and, when available, the spectrum of the most likely identification. For completeness we show here also the spectra of the previously known, optically selected AGNs already published in Zitelli et al. (1992). For all sources the optical images ( $1' \times 1'$ ) are taken from R CCDs, except for sources X046–03, X240–09 and X045–27, for which the images from the F plate are shown. The two circles drawn on the figures correspond to the 68% and 95% error boxes as defined above. The total number of objects in the 95% error boxes is  $\sim 140$ . Spectroscopy for such a large number of faint objects was obviously not possible, and therefore we had to decide a strategy for the follow-up spectroscopic observations of the most promising candidates. Our adopted strategy was the following:

i. First we have cross-correlated the positions of the 50 X-ray sources with those of the 29 optically selected AGNs previously known in the same area, finding 19 positional coincidences (see Section 2.1). With one exception (X019–17), all these AGNs have at least one of the two LR values higher than 1.6. We have considered them as likely identifications (these objects are indicated as **AGN**<sup>(1)</sup> in the last column of Table 3) and we decided not to observe spectroscopically other objects in these error boxes, including the X-ray source X019–17 in which the AGN has a relatively low likelihood ratio. We note here that our LR values are based only on optical magnitudes and morphology and do not take into account the spectroscopic information. At the typical magnitudes of the optical counterparts identified with AGNs ( $21 \leq m_B \leq 23$ ) the ratio between the number of objects classified as point-like objects in our CCD data and that of broad-line AGNs (Mignoli and Zamorani 1998) is in the range 10–15. Therefore, the “a posteriori” LR, when an AGN is found spectroscopically in any given error box, would be about 10–15 times higher than that listed in Table 3.

ii. Since AGNs are well known to be the dominant optical counterpart of faint X-ray sources, at least for  $S_x \geq 5 \times 10^{-15} \text{ erg cm}^{-2} \text{ s}^{-1}$ , we have then searched our optical catalogs for all the stellar or slightly fuzzy objects within the remaining 31 X-ray error boxes. We have then taken spectra for these objects helping us in making a priority list in each error box with additional

information from the colours, the magnitude and the distance between the objects and the X-centroid (i.e. the LR value). In addition to the objects that on the basis of these data were considered to be the most likely AGN candidates, we gave high priority also to objects which coincide with a radio source (see Table 2) and to objects with colours typical of M stars, which are the dominant spectral type of stars found in faint X-ray surveys. M stars with the highest ratio between X-ray and optical fluxes and with an X-ray flux equal to our limiting flux are expected to have at most an optical magnitude of the order of  $m_V \sim 19.75 \pm 0.25$  (see Maccacaro et al. 1988), corresponding to  $m_B \sim 21.25 \pm 0.25$ . From our own colour – colour diagrams (see also Marano et al. 1988) we estimate that the surface density of M stars with this limiting magnitude is  $\sim 380$  per square degree, in good agreement (within 15%) with the predictions of the Bahcall and Soneira model for the structure of the Galaxy (see, for example, Ratnatunga and Bahcall 1985). Following this recipe, we found spectroscopically four stars (two M stars with  $m_b \sim 19.5$  (X030–15 and X028–33), and two very bright F stars with  $m_b \sim 10$  (X046–03 and X045–27)), eight broad-line AGNs (X012–02, X042–11, X040–32, X032–36, X251–37, X024–38, X015–39, X306–42) and two radio galaxies (X021–05 and X409–28), one of which with broad MgII line. The blue magnitudes of the AGNs and the two radio galaxies are in the range 21.7 – 23.7.

We also took a spectrum for the relatively bright object ( $m_B = 21.44$ ), with LR values greater than 5.5, which is right at the center of the error box of source X051–43. Its spectrum does not show any clear evidence for convincing emission or absorption features, so that, even if we do consider it as the likely counterpart of the X-ray source, we have not been able to spectroscopically classify it. The absence of features in the spectrum suggests that it might be a BL Lac object. If so, it would be a somewhat anomalous BL Lac object. In fact, being not detected in the radio at a flux limit of about 0.2 mJy, it would be classified as a radio quiet BL Lac, with a radio to optical spectral index  $\alpha_{ro} < 0.26$ . None of the X-ray selected BL Lac objects in the Einstein Medium Sensitivity Survey (Stoche et al. 1991), and just a few in the much larger samples of ROSAT selected BL Lacs (see, for example, Perlman et al. 1998) have such a low value of  $\alpha_{ro}$ .

The LR values for most of these 15 suggested identifications are greater than 1 and are the highest in their error boxes. The only exceptions are the broad-line radio-galaxy identified with the source X409–28 and the AGN identified with the source X032–36, whose LR values are of the order of 0.5. In the latter error box there is also a brighter stellar object with higher LR values. However, its spectrum shows that it is a B type star and its identification with the X-ray source can therefore be excluded on the basis of the  $f_x/f_v$  ratio (Maccacaro et al. 1988). A few other objects have been observed spectroscopically in these 15 error boxes (see last column in Table 3) and

most of them have been found to be narrow emission line galaxies (NELG) or starburst galaxies. In all cases their LR value is significantly smaller than that of the best candidate and therefore we consider them unlikely to be associated to the X-ray sources. The estimated surface densities of AGNs with  $m_B \leq 23.5$  ( $\sim 325$  per square degree, Mignoli and Zamorani 1998) is similar to the surface density of M stars with  $m_V < 20$ . From the sum of the two surface densities we estimate that only  $\sim 0.7$  random coincidences in the 95% error circles of the 31 X-ray sources are expected for AGNs and M stars in the magnitude ranges covered by these suggested identifications.

iii. For the 16 error boxes which at this stage were still without a reliable optical identification, we have taken spectra also of objects classified as extended. At the typical magnitudes of the optical counterparts ( $m_B > 22.0$ ) the surface density of objects classified as extended in our optical images is higher than that of stellar objects. The ratio between the numbers of extended and stellar objects in our CCD catalogue is  $\sim 2$  at  $m_B \sim 22.25$  and  $\sim 5$  at  $m_B \sim 23.25$ . Therefore, the large number of extended objects makes more difficult to deal with the problem of random coincidences and to find convincing optical identifications. Each of these sixteen error boxes is now discussed in some detail, in order of decreasing X-ray flux.

**X043–12:** the 95% error box contains only one object, classified as extended in the blue band and as point-like in the V and R bands. Its noisy spectrum shows two narrow lines well coincident with Ly $\alpha$  and CIV at  $z = 2.80$ . It appears to be a high redshift analogue of the low- $z$  type-2 AGNs, similar to the QSO 2 at  $z = 2.35$  found by Almaini et al. (1995) in the optical follow-up of other deep ROSAT fields. Although a higher quality spectrum would be needed to confirm the nature of this object, given its relatively large LR values, we consider it as the correct identification.

**X039–19** and **X049–21:** these are the brightest X-ray sources in our sample without any suggested spectroscopic identification. The 95% error box of X039–19 does not contain any object in our CCD data, while a faint ( $m_B \sim 24$ ), extended object is present near the center of the error box of X049–21. Its relatively large LR values suggest that it might be the correct optical identification. However, both the spectrum of this object (shown in figure 4) and the spectrum of a similarly faint object just outside the error box of X039–19 (object A in figure 4) have extremely low S/N and do not allow any spectroscopic classification. Moreover, both X-ray sources have a close-by source at less than one arcmin (see figure 1), so that it is possible that their X-ray positions are not as well determined as those of the other sources with similar X-ray flux.

**X211–22:** we took spectra for three objects, all of them just outside the 95% radius. The brightest one is an early type galaxy at  $z = 0.180$ , while the other two, separated by about 2 arcsec from each other, are a Sey 1 galaxy (classified as point-like in the B band and as

**Table 3.** The Optical Data

| ID.     | $\Delta\alpha$<br>["] | $\Delta\delta$<br>["] | $\Delta''/\frac{\Delta}{\epsilon_x}$ | $m_B$   | $m_R$  | U-B    | B-V    | V-R    | $LR_B$ | $LR_R$ | z     | object notes                   |
|---------|-----------------------|-----------------------|--------------------------------------|---------|--------|--------|--------|--------|--------|--------|-------|--------------------------------|
| X013-01 | 1.2                   | -0.0                  | 1.2/0.8                              | >25.00  | 23.17  |        |        | > 1.13 | e      | 4.73   |       |                                |
|         | -4.0                  | -1.7                  | 4.3/2.8                              | 19.96   | 19.61  | -0.55  | -0.09  | 0.44   | p      | 1.25   | 1.63  | 1.663 <b>AGN<sup>(1)</sup></b> |
| X012-02 | -7.6                  | 0.2                   | 7.6/2.8                              | 21.94   | 20.58  | -0.70  | 0.63   | 0.73   | p      | 1.16   | 0.65  | 1.378 <b>AGN</b>               |
| X046-03 | -1.4                  | 0.9                   | 1.6/1.0                              | ~9.3    |        |        | ~0.5   |        |        |        | 0.00  | <b>F6IV star</b>               |
| X036-04 | -0.4                  | -0.3                  | 0.5/0.2                              | 18.04*  | 17.07  | -0.78  | 0.55   | 0.42   | p      | 17.86  | 28.60 | 2.531 <b>AGN<sup>(1)</sup></b> |
|         | 0.8                   | 5.1                   | 5.1/2.1                              | >23.50* | 23.44  |        | >-0.67 | 0.73   | e      | 0.29   |       |                                |
| X021-05 | -2.7                  | 0.0                   | 2.7/1.5                              | 21.79   | 19.28  | 0.66   | 1.48   | 1.03   | e      | 6.83   | 3.58  | 0.387 <b>RadioGal</b>          |
| X025-06 | 1.0                   | -1.6                  | 1.9/1.0                              | 21.43   | 20.97  | -0.52  | 0.36   | 0.10   | p      | 71.44  | 45.19 | 0.808 <b>AGN<sup>(1)</sup></b> |
| X027-07 | 3.0                   | 3.3                   | 4.4/2.0                              | 21.17   | 20.66  | -0.55  | 0.19   | 0.32   | p      | 11.89  | 7.52  | 0.636 <b>AGN<sup>(1)</sup></b> |
|         | -3.4                  | -5.6                  | 6.6/2.9                              | 23.34   | 22.87  | -0.86  | 0.29   | 0.18   | e      | 0.12   | 0.09  |                                |
| X041-08 | 1.8                   | 3.6                   | 4.0/1.5                              | 21.62   | 21.06  | -0.67  | 0.35   | 0.21   | p      | 20.74  | 10.78 | 2.161 <b>AGN<sup>(1)</sup></b> |
|         | -3.5                  | -5.7                  | 6.7/2.6                              | 24.04   | 23.46  | -0.66  | 0.41   | 0.17   | e      | 0.08   | 0.08  |                                |
|         | 0.3                   | -7.5                  | 7.5/2.9                              | 24.20   | >23.50 | >-0.70 | 0.48   | < 0.22 | e      | 0.04   |       |                                |
|         | -8.5                  | 2.3                   | 8.8/3.4                              | 24.15   | >23.50 | >-0.65 | -0.21  | < 0.86 | e      | 0.01   |       |                                |
| X240-09 | -0.3                  | 4.0                   | 4.0/1.0                              | 21.81*  | 20.87* | -0.71  | 0.52   | 0.42   | p      | 17.75  | 9.99  | 0.854 <b>AGN<sup>(1)</sup></b> |
|         | 12.4                  | -1.9                  | 12.5/3.2                             | 22.54*  | 21.91* | -0.74  | 0.34   | 0.29   | e      | 0.01   | 0.02  |                                |
| X033-10 | 7.2                   | 1.4                   | 7.3/1.7                              | 21.90*  | 20.91  | -0.90  | 0.65   | 0.34   | p      | 5.70   | 3.21  | 0.983 <b>AGN<sup>(1)</sup></b> |
|         | 1.0                   | 12.6                  | 12.6/3.0                             | >23.50* | 21.86  |        | > 0.72 | 0.92   | p      | 0.09   |       |                                |
| X042-11 | -0.8                  | 2.4                   | 2.5/1.1                              | 22.99   | 22.04  | -0.33  | 0.58   | 0.37   | p/e    | 19.50  | 5.43  | 1.062 <b>AGN</b>               |
|         | -6.8                  | -3.8                  | 7.8/3.3                              | -out-   | 22.10  |        |        | 1.00   | e      | 0.04   |       |                                |
| X043-12 | 1.6                   | 3.1                   | 3.5/1.5                              | 23.80   | 22.61  | -0.32  | 0.17   | 1.02   | e/p    | 1.66   | 0.87  | 2.80: <b>AGN2 (?)</b>          |
|         | 5.3                   | -5.8                  | 7.9/3.4                              | 24.15   | 22.93  | -0.47  | 0.95   | 0.27   | e      | 0.01   | 0.02  |                                |
| X023-13 | 0.3                   | -0.7                  | 0.8/0.3                              | 22.24   | 21.99  | -0.45  | -0.10  | 0.35   | p      | 36.47  | 19.86 | 1.573 <b>AGN<sup>(1)</sup></b> |
|         | 4.5                   | -8.1                  | 9.3/3.4                              | 23.94   | 21.32  | >-0.44 | 1.42   | 1.20   | e      | 0.01   | 0.02  |                                |
| X108-14 | 3.6                   | 0.6                   | 3.6/0.8                              | 22.42   | 21.63  | -1.55  | 0.23   | 0.56   | p      | 10.04  | 5.47  | 1.374 <b>AGN<sup>(1)</sup></b> |
|         | -4.8                  | 3.1                   | 5.7/1.3                              | 21.30   | 20.36  | 0.05   | 0.52   | 0.42   | e      | 2.90   | 1.71  |                                |
| X030-15 | 0.5                   | 3.5                   | 3.6/0.8                              | 24.07   | >23.50 | -0.35  | <-0.23 |        | p      | 0.60   |       |                                |
|         | 0.5                   | 7.6                   | 7.6/1.8                              | 19.28   | 16.86  | 1.20   | 1.59   | 0.83   | p      | 1.95   | 2.59  | 0.00 <b>M star</b>             |
|         | -8.1                  | 10.1                  | 13.0/3.0                             | 23.29   | 22.20  | -0.11  | 0.87   | 0.22   | e      | 0.02   | 0.03  |                                |
|         | -13.0                 | -5.7                  | 14.2/3.3                             | 22.99   | 22.24  | -0.86  | 0.33   | 0.42   | e      | 0.01   | 0.01  |                                |
| X304-16 | -1.0                  | 1.6                   | 1.9/0.6                              | 21.53   | 20.73  | -0.74  | 0.39   | 0.41   | p      | 39.05  | 21.97 | 1.192 <b>AGN<sup>(1)</sup></b> |
|         | -2.6                  | 5.7                   | 6.3/2.0                              | 24.04   | 23.05  | -0.84  | 0.40   | 0.59   | e      | 0.21   | 0.21  |                                |
|         | 9.8                   | -2.2                  | 10.1/3.2                             | 23.59   | 22.27  | -0.70  | 0.46   | 0.86   | e      | 0.02   | 0.03  |                                |
| X019-17 | 0.9                   | -2.8                  | 2.9/0.8                              | 24.34   | 23.47  | -0.90  | 0.78   | 0.09   | e      | 0.85   | 0.85  |                                |
|         | -2.8                  | 8.7                   | 9.2/2.5                              | 23.45   | 21.20  | > 0.05 | 1.35   | 0.90   | p      | 0.30   | 0.74  |                                |
|         | -5.5                  | -10.4                 | 11.7/3.2                             | 22.40*  | 21.69  | -0.70  | 0.49   | 0.22   | p/e    | 0.12   | 0.03  | 0.614 <b>AGN<sup>(1)</sup></b> |
| X029-18 | 3.5                   | 4.8                   | 6.0/1.6                              | 23.67   | 21.94  | -0.10  | 1.11   | 0.62   | e      | 0.56   | 1.20  |                                |
|         | 0.9                   | -6.2                  | 6.2/1.6                              | 21.66   | 21.15  | -1.01  | 0.23   | 0.28   | p      | 8.42   | 4.37  | 1.254 <b>AGN<sup>(1)</sup></b> |
| X039-19 | -10.5                 | 2.2                   | 10.7/3.3                             | 23.63   | 22.41  | -0.20  | 0.99   | 0.23   | e      | 0.01   | 0.02  | ???? low S/N (A)               |
| X001-20 | -5.4                  | -1.8                  | 5.7/1.6                              | 20.39   | 19.71  | -0.83  | 0.26   | 0.42   | p      | 2.31   | 3.92  | 1.353 <b>AGN<sup>(1)</sup></b> |
|         | -8.4                  | 7.0                   | 10.9/3.0                             | 22.72   | 22.73  | -1.00  | -0.09  | 0.08   | p      | 0.16   | 0.01  |                                |
| X049-21 | -3.2                  | -1.7                  | 3.6/1.2                              | 23.86   | 22.36  | -0.61  | 0.68   | 0.82   | e      | 1.50   | 2.82  | ???? low S/N                   |
| X211-22 | -0.2                  | -6.9                  | 6.9/1.6                              | 24.27   | 23.31  | -0.51  | <-0.03 | > 0.99 | e      | 0.23   | 0.23  |                                |
|         | 9.3                   | 7.5                   | 12.0/2.8                             | 20.97   | 19.35  | 0.11   | 1.06   | 0.56   | e      | 0.07   | 0.04  | 0.180 early gal                |
|         | -12.5                 | 0.5                   | 12.5/2.9                             | 22.20   | 20.26  | -0.45  | 0.86   | 1.08   | p/e    | 0.23   | 0.07  | 0.281 <b>AGN (Sy 1)</b>        |
|         | -12.3                 | -4.0                  | 13.0/3.0                             | 24.37   | 22.99  | -0.16  | 0.43   | 0.95   | e      | 0.01   | 0.02  |                                |
|         | -13.5                 | 0.1                   | 13.5/3.1                             | 22.12   | 21.36  | -0.04  | 0.41   | 0.35   | p      | 0.12   | 0.10  | 0.00 B star                    |
|         | 7.0                   | 12.9                  | 14.7/3.4                             | 24.60   | 23.49  | >-1.10 | 0.64   | 0.47   | e      | 0.00   | 0.00  |                                |



| ID.     | $\Delta\alpha$<br>["] | $\Delta\delta$<br>["] | $\Delta''/\frac{\Delta}{\epsilon_x}$ | $m_B$   | $m_R$  | U-B    | B-V    | V-R    | $LR_B$ | $LR_R$ | z     | object notes |                    |
|---------|-----------------------|-----------------------|--------------------------------------|---------|--------|--------|--------|--------|--------|--------|-------|--------------|--------------------|
| X404-23 | 11.8                  | -1.4                  | 11.9/1.3                             | 24.03   | 22.74  | >-0.53 | 0.70   | 0.59   | e      | 0.08   | 0.17  |              |                    |
|         | 6.0                   | 10.9                  | 12.4/1.3                             | >25.00  | 23.25  |        |        | > 1.05 | e      |        | 0.07  |              |                    |
|         | -9.8                  | -10.1                 | 14.1/1.5                             | 23.67   | 22.54  | -0.38  | 0.87   | 0.26   | e      | 0.10   | 0.12  |              |                    |
|         | -16.1                 | -1.6                  | 16.2/1.7                             | 24.25   | 22.67  | >-0.75 | 0.76   | 0.82   | e      | 0.04   | 0.09  |              |                    |
|         | 6.2                   | -16.5                 | 17.6/1.9                             | 24.47   | 23.41  | >-0.97 | 0.26   | 0.80   | e      | 0.03   | 0.03  |              |                    |
|         | 8.9                   | -16.5                 | 18.8/2.0                             | 24.89   | 23.18  | >-1.39 | 0.70   | 1.01   | e      | 0.01   | 0.02  |              |                    |
|         | -12.9                 | -15.5                 | 20.2/2.2                             | 23.40   | 22.34  | -0.77  | 0.57   | 0.49   | e      | 0.05   | 0.06  | 0.204        | NELG (G)           |
|         | -18.0                 | -9.3                  | 20.3/2.2                             | 24.23   | 23.60  | -0.17  | 0.16   | 0.47   | e      | 0.02   | 0.01  |              |                    |
|         | -3.7                  | 21.3                  | 21.6/2.3                             | 24.32   | 23.47  | -0.66  | 0.41   | 0.44   | e      | 0.01   | 0.01  |              |                    |
|         | 11.9                  | -19.3                 | 22.6/2.4                             | 23.55   | 21.01  | >-0.05 | 1.31   | 1.23   | p      | 0.03   | 0.14  | 0.00         | M star (J)         |
|         | 23.3                  | 14.2                  | 27.3/2.9                             | 23.65   | 21.81  | >-0.15 | 0.85   | 0.99   | e      | 0.00   | 0.01  |              |                    |
|         | 24.6                  | -12.6                 | 27.7/3.0                             | 23.80   | 22.20  | -1.18  | 0.75   | 0.85   | e      | 0.00   | 0.01  |              |                    |
|         | 24.1                  | 13.7                  | 27.7/3.0                             | 23.82   | >23.50 | >-0.32 | -0.24  | < 0.56 | e      | 0.00   |       |              |                    |
|         | 13.6                  | -24.3                 | 27.8/3.0                             | 23.67   | 23.04  | -0.67  | -0.16  | 0.79   | e      | 0.00   | 0.00  |              |                    |
|         | 27.8                  | -5.3                  | 28.3/3.0                             | 22.51   | 21.70  | -0.36  | 0.52   | 0.29   | e      | 0.00   | 0.01  | 0.157        | Sy2 (?) (N)        |
|         | -27.1                 | 8.9                   | 28.5/3.1                             | 23.76   | 21.43  | >-0.26 | 1.28   | 1.05   | p      | 0.01   | 0.02  |              |                    |
|         | -15.7                 | 24.5                  | 29.1/3.1                             | >25.00  | 23.35  |        | > 0.77 | 0.88   | e      |        | 0.00  |              |                    |
| 8.3     | 28.2                  | 29.4/3.2              | 24.45                                | 21.94   | >-0.95 | 1.51   | 1.00   | p      | 0.00   | 0.01   |       |              |                    |
| X031-24 | 0.0                   | 2.8                   | 2.8/0.6                              | 21.37*  | 20.71  | -0.72  | 0.32   | 0.34   | p      | 17.50  | 11.07 | 0.409        | AGN <sup>(1)</sup> |
|         | -1.3                  | -3.7                  | 3.9/0.9                              | >23.50* | 21.23  |        | > 1.19 | 1.08   | e      |        | 1.90  |              |                    |
|         | 5.8                   | 1.0                   | 5.9/1.4                              | >23.50* | 23.18  |        | >-0.77 | 1.09   | e      |        | 0.33  |              |                    |
|         | -0.9                  | -7.8                  | 7.8/1.8                              | >23.50* | 21.71  |        | > 1.37 | 0.42   | e      |        | 0.64  |              |                    |
|         | 0.1                   | -13.6                 | 13.6/3.1                             | >23.50* | 22.82  |        | > 0.21 | 0.47   | e      |        | 0.01  |              |                    |
| X050-25 | -0.4                  | 0.7                   | 0.8/0.2                              | 20.77   | 20.39  | -0.72  | 0.04   | 0.34   | p      | 18.47  | 13.93 | 1.315        | AGN <sup>(1)</sup> |
|         | 4.0                   | -5.8                  | 7.1/1.9                              | 24.17   | 23.08  | >-0.67 | 0.31   | 0.78   | e      | 0.19   | 0.19  |              |                    |
| X235-26 | -0.9                  | -1.7                  | 1.9/0.4                              | 21.40   | 20.96  | -0.00  | 0.26   | 0.18   | p      | 13.94  | 8.82  | 2.536        | AGN <sup>(1)</sup> |
|         | 2.5                   | -1.0                  | 2.7/0.5                              | 24.92   | 23.42  | >-1.42 | < 0.62 | > 0.88 | e      | 0.23   | 0.50  |              |                    |
|         | -0.5                  | -5.2                  | 5.2/1.0                              | 22.28   | 20.88  | -0.42  | 0.69   | 0.71   | e      | 1.54   | 1.24  |              |                    |
|         | 5.5                   | -9.5                  | 11.0/2.1                             | 23.37   | 22.14  | -0.62  | 0.57   | 0.66   | e      | 0.19   | 0.21  |              |                    |
|         | 2.7                   | 10.9                  | 11.2/2.1                             | 24.33   | 23.37  | >-0.83 | 0.40   | 0.56   | e      | 0.06   | 0.06  |              |                    |
|         | -10.5                 | -9.7                  | 14.3/2.7                             | 24.46   | 23.73  | -0.64  | 0.03   | 0.70   | e      | 0.01   | 0.01  |              |                    |
|         | 7.6                   | 14.9                  | 16.8/3.2                             | >25.00  | 22.55  |        | > 0.88 | 1.57   | e      |        | 0.01  |              |                    |
| 11.6    | -13.4                 | 17.7/3.4              | 23.45                                | 22.10   | 0.08   | 0.49   | 0.86   | e      | 0.01   | 0.01   |       |              |                    |
| X045-27 | 2.6                   | -9.8                  | 10.1/2.9                             | ~10.0   |        |        | ~0.3   |        |        |        | 0.00  | F5V star     |                    |
| X409-28 | 0.1                   | -7.5                  | 7.5/1.4                              | 23.70   | 21.81  | -0.65  | 0.97   | 0.92   | e      | 0.36   | 0.79  | 0.957        | AGN (BLRG)         |
|         | -6.5                  | 5.0                   | 8.2/1.6                              | 24.67   | >23.50 | >-1.17 | < 0.37 |        | e      | 0.10   |       |              |                    |
|         | -9.0                  | -3.1                  | 9.5/1.8                              | 24.46   | 23.21  | -0.78  | 0.24   | 1.01   | e      | 0.11   | 0.11  |              |                    |
|         | 3.5                   | -9.3                  | 9.9/1.9                              | 24.27   | 22.47  | >-0.77 | 0.87   | 0.93   | e      | 0.09   | 0.32  |              |                    |
|         | -6.5                  | -8.6                  | 10.7/2.0                             | >25.00  | 22.76  |        |        | > 1.54 | e      |        | 0.15  |              |                    |
|         | -10.1                 | -6.6                  | 12.1/2.3                             | 23.65   | 22.68  | -0.66  | 0.41   | 0.56   | e      | 0.07   | 0.08  |              |                    |
|         | 13.5                  | 5.6                   | 14.6/2.8                             | 24.41   | 23.50  | -0.56  | 0.29   | 0.62   | e      | 0.01   | 0.00  |              |                    |
| X301-29 | -2.5                  | 0.4                   | 2.6/0.6                              | 21.13*  | 20.41* | -0.88  | 0.40   | 0.32   | p      | 19.92  | 10.18 | 1.709        | AGN <sup>(1)</sup> |
|         | -0.9                  | 5.9                   | 6.0/1.5                              | 23.86   | 22.67  | -0.42  | 0.56   | 0.63   | e      | 0.57   | 0.68  |              |                    |
|         | -2.7                  | -10.4                 | 10.8/2.6                             | 19.13*  | 16.30* | 1.09   | 1.59   | 1.24   | p      | 0.32   | 0.25  |              |                    |
|         | 4.7                   | 11.3                  | 12.2/3.0                             | 22.79   | 21.13  | -1.38  | 0.96   | 0.70   | e      | 0.03   | 0.04  |              |                    |
| X408-30 | -9.6                  | 3.5                   | 10.2/2.5                             | 24.76   | >23.50 | >-1.26 | 0.40   | < 0.86 | e      | 0.02   |       |              |                    |
|         | 12.8                  | 5.9                   | 14.1/3.4                             | 24.56   | 23.00  | >-1.06 | 0.70   | 0.86   | e      | 0.00   | 0.00  |              |                    |
|         | 4.6                   | 13.8                  | 14.6/3.6                             | 23.49   | 21.53  | -0.30  | 1.04   | 0.92   | e      | 0.00   | 0.01  | 0.814        | NELG (C)           |
| X207-31 | -5.7                  | -0.7                  | 5.7/1.2                              | 23.37   | 22.19  | -0.38  | 0.64   | 0.54   | e      | 0.98   | 1.11  |              |                    |
|         | -1.6                  | -8.0                  | 8.1/1.7                              | 23.78   | 22.43  | -0.44  | 0.84   | 0.51   | e      | 0.29   | 0.56  | 0.58:        | cluster gal        |
|         | -10.0                 | 4.8                   | 11.1/2.3                             | 24.05   | 22.97  | >-0.55 | 0.44   | 0.64   | e      | 0.05   | 0.11  |              |                    |
|         | -6.7                  | 10.0                  | 12.0/2.5                             | 24.58   | 23.55  | >-1.08 | 0.45   | 0.58   | e      | 0.02   | 0.02  |              |                    |
|         | -12.3                 | 1.0                   | 12.3/2.5                             | >25.00  | 23.22  |        |        | > 1.08 | e      |        | 0.03  |              |                    |
|         | -14.0                 | -5.8                  | 15.2/3.1                             | 24.58   | >23.50 | >-1.08 | < 0.28 |        | e      | 0.00   |       |              |                    |
|         | -15.7                 | 6.4                   | 16.9/3.5                             | 23.94   | 22.38  | -0.43  | 0.57   | 0.99   | e      | 0.00   | 0.01  |              |                    |
|         | -5.8                  | 17.3                  | 18.2/3.7                             | 24.34   | 23.69  | -0.84  | 0.11   | 0.54   | e      | 0.00   | 0.00  |              |                    |
|         | -17.3                 | -6.3                  | 18.5/3.8                             | 22.68   | 19.65  | > 0.82 | 1.72   | 1.31   | e      | 0.00   | 0.00  | 0.584        | cD gal             |

| ID.     | $\Delta\alpha$<br>[ $''$ ] | $\Delta\delta$<br>[ $''$ ] | $\Delta'' / \frac{\Delta}{\epsilon_x}$ | $m_B$  | $m_R$  | U-B    | B-V    | V-R    | $LR_B$ | $LR_R$ | z     | object notes         |                       |
|---------|----------------------------|----------------------------|--|--------|--------|--------|--------|--------|--------|--------|-------|----------------------|-----------------------|
| X040-32 | 6.0                        | 2.6                        | 6.6/1.9                                | 23.37  | 22.31  | -0.68  | 0.57   | 0.49   | p      | 1.30   | 0.99  | 1.204                | <b>AGN</b>            |
|         | -6.1                       | 4.8                        | 7.8/2.2                                | 24.53  | >23.50 | -0.82  | -0.30  | < 1.33 | e      | 0.08   |       |                      |                       |
|         | 8.3                        | 1.5                        | 8.4/2.4                                | 23.26  | 21.99  | -0.74  | 0.52   | 0.75   | e      | 0.21   | 0.27  | 0.804                | NELG                  |
|         | 9.0                        | 4.1                        | 9.8/2.8                                | 23.61  | 22.27  | 0.41   | 0.52   | 0.82   | e      | 0.04   | 0.08  |                      |                       |
| X028-33 | -3.1                       | -0.0                       | 3.1/0.6                                | >25.00 | >23.50 | <-1.77 |        |        | p      |        |       |                      |                       |
|         | 4.3                        | -0.3                       | 4.3/0.9                                | 23.20  | 22.20  | -0.78  | 0.40   | 0.60   | e      | 1.35   | 1.53  |                      |                       |
|         | -5.5                       | -1.8                       | 5.8/1.2                                | 19.16  | 17.22  | 1.06   | 1.29   | 0.65   | p      | 3.64   | 3.59  | 0.00                 | <b>M star</b>         |
|         | -1.8                       | -10.7                      | 10.8/2.3                               | 21.95  | 20.98  | -0.61  | 0.36   | 0.61   | e      | 0.23   | 0.19  | 0.657                | NELG                  |
|         | 11.1                       | -4.4                       | 11.9/2.5                               | 23.88  | 23.32  | -0.79  | 0.28   | 0.28   | e      | 0.06   | 0.03  |                      |                       |
|         | 12.2                       | 8.0                        | 14.6/3.0                               | 23.89  | 23.01  | -0.43  | 0.10   | 0.78   | p      | 0.02   | 0.01  |                      |                       |
|         | 16.0                       | 1.8                        | 16.1/3.4                               | 24.25  | 21.71  | >-0.75 | 1.26   | 1.28   | e      | 0.00   | 0.01  |                      |                       |
| X250-34 | 7.1                        | 0.6                        | 7.1/1.6                                | 24.30  | 23.59  | >-0.80 | < 0.00 | > 0.71 | e      | 0.22   | 0.16  |                      |                       |
|         | -8.9                       | 5.6                        | 10.5/2.4                               | 23.29  | 22.94  | > 0.21 | 0.08   | 0.27   | e      | 0.13   | 0.10  |                      |                       |
|         | -9.1                       | -6.0                       | 10.9/2.5                               | 24.32  | 23.68  | >-0.82 | < 0.02 | > 0.62 | e      | 0.04   | 0.02  |                      |                       |
|         | 6.8                        | -8.9                       | 11.2/2.6                               | >25.00 | 23.18  |        |        | > 1.12 | e      |        | 0.03  |                      |                       |
| X011-35 | 0.6                        | -0.8                       | 1.0/0.2                                | 21.94  | 20.33  | -0.20  | 1.14   | 0.47   | e      | 1.80   | 2.03  | 0.189                | abs.gal (A)           |
|         | 1.7                        | 2.5                        | 3.1/0.5                                | 24.49  | 23.75  | >-0.99 | < 0.19 | > 0.55 | e      | 0.37   | 0.23  |                      |                       |
|         | 0.8                        | 6.3                        | 6.4/1.0                                | 23.61  | 22.40  | -0.32  | 0.63   | 0.58   | e      | 0.43   | 0.81  |                      |                       |
|         | -7.8                       | 5.5                        | 9.5/1.6                                | 21.95  | 20.63  | -0.67  | 0.76   | 0.56   | e      | 0.54   | 0.44  | 0.391                | <b>NELG</b> (D)       |
|         | -7.6                       | -5.8                       | 9.6/1.6                                | 23.99  | >23.50 | >-0.49 | -0.19  | < 0.68 | e      | 0.22   |       |                      |                       |
|         | -1.0                       | -10.2                      | 10.2/1.7                               | 24.03  | 21.34  | >-0.53 | 1.34   | 1.35   | e      | 0.10   | 0.36  | 0.586                | early gal (F)         |
|         | 7.3                        | -7.4                       | 10.4/1.7                               | 24.02  | 23.42  | -0.97  | -0.05  | 0.65   | p      | 0.10   | 0.10  |                      |                       |
|         | -11.9                      | 0.2                        | 11.9/1.9                               | 23.63  | 22.94  | >-0.13 | 0.39   | 0.30   | e      | 0.11   | 0.14  |                      |                       |
|         | -6.0                       | -12.0                      | 13.4/2.2                               | 22.52  | 21.29  | -0.39  | 0.64   | 0.59   | e      | 0.09   | 0.13  | ?..???               | low S/N (I)           |
|         | -10.0                      | -10.9                      | 14.8/2.4                               | 23.45  | 23.63  | > 0.05 | 0.05   | -0.23  | e      | 0.07   | 0.02  |                      |                       |
|         | 7.4                        | -16.9                      | 18.5/3.0                               | 24.72  | 22.17  | >-1.22 | 1.41   | 1.14   | p      | 0.00   | 0.02  |                      |                       |
|         | -15.0                      | 13.4                       | 20.1/3.3                               | 22.00  | 20.15  | > 1.00 | 1.14   | 0.71   | e      | 0.01   | 0.01  | 0.390                | <b>early+[OII](L)</b> |
|         | -4.8                       | -21.2                      | 21.7/3.5                               | 24.02  | 22.66  | >-0.52 | 0.90   | 0.46   | e      | 0.00   | 0.00  |                      |                       |
| -19.5   | 10.9                       | 22.3/3.6                   | -out-                                  | 22.86  |        |        | 0.93   | e      |        | 0.00   |       |                      |                       |
| 8.9     | -22.3                      | 24.0/3.9                   | 22.90                                  | 20.57  | > 0.60 | 1.31   | 1.02   | e      | 0.00   | 0.00   | 0.390 | <b>early gal</b> (O) |                       |
| X032-36 | 5.3                        | -3.1                       | 6.1/1.1                                | 24.43  | 23.19  | >-0.93 | 0.51   | 0.73   | e      | 0.28   | 0.28  |                      |                       |
|         | -3.8                       | 9.4                        | 10.1/1.9                               | 24.24  | 22.81  | >-0.74 | 0.87   | 0.56   | e      | 0.09   | 0.20  |                      |                       |
|         | 4.4                        | 9.2                        | 10.3/1.9                               | 21.26  | 20.61  | -0.15  | 0.34   | 0.31   | p      | 2.27   | 1.44  | 0.00                 | B star                |
|         | 0.5                        | 12.4                       | 12.4/2.3                               | 23.36  | 21.98  | -0.56  | 0.79   | 0.59   | p      | 0.54   | 0.37  | 1.190                | <b>AGN</b>            |
|         | 10.6                       | 9.0                        | 13.9/2.6                               | >25.00 | 22.88  |        | > 1.09 | 1.03   | e      |        | 0.04  |                      |                       |
|         | -0.2                       | -14.3                      | 14.3/2.6                               | 24.21  | 23.46  | >-0.71 | 0.66   | 0.09   | p      | 0.02   | 0.02  |                      |                       |
|         | -8.9                       | -13.4                      | 16.1/3.0                               | 24.21  | 23.43  | >-0.71 | 0.22   | 0.56   | e      | 0.01   | 0.01  |                      |                       |
|         | 16.3                       | 1.6                        | 16.4/3.0                               | >25.00 | 23.27  |        |        | > 1.03 | e      |        | 0.01  |                      |                       |
| X251-37 | -6.1                       | 4.5                        | 7.6/1.3                                | 21.72  | 20.68  | -0.20  | 0.70   | 0.34   | p      | 5.70   | 3.20  | 2.710                | <b>AGN</b>            |
|         | 4.3                        | 6.9                        | 8.1/1.3                                | 24.34  | 23.40  | >-0.84 | 0.57   | 0.37   | e      | 0.17   | 0.17  |                      |                       |
|         | 3.5                        | 12.4                       | 12.9/2.1                               | 24.61  | >23.50 | >-1.11 | < 0.31 |        | e      | 0.03   |       |                      |                       |
|         | -13.7                      | 0.8                        | 13.7/2.3                               | 20.03  | 18.40  | 0.28   | 1.07   | 0.56   | e      | 0.23   | 0.14  | 0.091                | early gal             |
|         | -12.3                      | 8.0                        | 14.7/2.4                               | 23.95  | 22.80  | >-0.45 | 0.81   | 0.34   | e      | 0.04   | 0.05  |                      |                       |
| X024-38 | 0.8                        | -0.0                       | 0.8/0.1                                | 22.19  | 20.76  | -0.37  | 0.77   | 0.66   | p      | 9.29   | 8.72  | 1.430                | <b>AGN</b>            |
|         | 3.6                        | -3.6                       | 5.1/0.9                                | 17.94  | 16.82  | 0.02   | 0.45   | 0.67   | p      | 3.39   | 5.06  | 0.00                 | B star                |
|         | 0.4                        | 9.3                        | 9.3/1.7                                | 23.21  | 22.23  | -0.24  | 0.73   | 0.25   | p      | 0.75   | 0.57  | 0.276                | NELG                  |
|         | 8.5                        | 10.1                       | 13.2/2.4                               | 22.76  | 21.26  | 0.24   | 0.88   | 0.62   | e      | 0.06   | 0.09  |                      |                       |
|         | 2.4                        | 15.8                       | 16.0/3.0                               | 23.82  | 23.54  | >-0.32 | 0.50   | -0.22  | e      | 0.01   | 0.01  |                      |                       |
|         | -17.4                      | -1.8                       | 17.5/3.2                               | 24.35  | 22.65  | >-0.85 | 0.95   | 0.75   | e      | 0.00   | 0.01  |                      |                       |
|         | 17.8                       | -2.1                       | 17.9/3.3                               | 14.59  | 13.36  | -0.54  | 0.23   | 1.00   | p      | 0.15   | 0.06  | 0.00                 | A star                |
|         | -19.1                      | -1.1                       | 19.1/3.5                               | 23.95  | >23.50 | >-0.45 | -0.34  | < 0.79 | e      | 0.00   |       |                      |                       |
|         | -10.1                      | 16.9                       | 19.7/3.6                               | 16.99  | 15.68  | 0.29   | 0.42   | 0.89   | p      | 0.00   | 0.00  | 0.00                 | G star                |
| X015-39 | -5.4                       | -5.8                       | 7.9/1.1                                | 23.27  | 22.01  | -0.46  | 0.69   | 0.57   | p      | 1.04   | 0.79  | 0.500                | <b>AGN (Sy 1)</b>     |
|         | 13.1                       | -8.1                       | 15.4/2.2                               | >25.00 | 23.22  |        |        | > 1.08 | e      |        | 0.03  |                      |                       |
|         | -17.4                      | -2.8                       | 17.6/2.5                               | 23.48  | 22.73  | -0.68  | 0.15   | 0.60   | e      | 0.04   | 0.03  |                      |                       |
|         | 7.2                        | -17.2                      | 18.7/2.7                               | 24.64  | 23.43  | >-1.14 | < 0.34 | > 0.87 | e      | 0.01   | 0.01  |                      |                       |
|         | -17.3                      | -7.5                       | 18.8/2.7                               | 23.85  | 22.62  | -0.79  | 0.21   | 1.02   | e      | 0.01   | 0.02  | ?..???               | low S/N               |

| ID.     | $\Delta\alpha$<br>["] | $\Delta\delta$<br>["] | $\Delta''/\frac{\Delta}{\epsilon_x}$ | $m_B$   | $m_R$  | U-B    | B-V    | V-R    | $LR_B$ | $LR_R$ | z    | object notes |                           |
|---------|-----------------------|-----------------------|--------------------------------------|---------|--------|--------|--------|--------|--------|--------|------|--------------|---------------------------|
| X236-40 | 5.6                   | -0.3                  | 5.6/1.3                              | 22.23*  | 21.64  | -1.00  | 0.24   | 0.35   | p      | 6.38   | 3.47 | 1.140        | <b>AGN</b> <sup>(1)</sup> |
|         | -7.7                  | 0.5                   | 7.7/1.8                              | >23.50* | 22.00  |        | > 0.11 | 1.39   | e      |        | 0.57 |              |                           |
|         | -8.7                  | -2.1                  | 8.9/2.1                              | 24.55   | 23.73  | >-1.05 | 0.19   | 0.63   | e      | 0.07   | 0.06 |              |                           |
|         | -12.0                 | -3.0                  | 12.4/2.9                             | >25.00  | 23.19  |        | > 0.39 | 1.42   | e      |        | 0.01 |              |                           |
|         | -6.2                  | 12.3                  | 13.8/3.2                             | 24.30   | 22.64  | -0.60  | 0.65   | 1.01   | e      | 0.00   | 0.01 |              |                           |
| X234-41 | 0.9                   | 1.2                   | 1.5/0.3                              | 23.38   | 22.18  | 0.17   | 0.77   | 0.43   | e      | 1.58   | 1.78 |              |                           |
|         | -0.5                  | 4.1                   | 4.1/0.8                              | 23.83   | 23.29  | -0.54  | -0.03  | 0.57   | e      | 0.73   | 0.41 |              |                           |
|         | 1.5                   | -4.1                  | 4.3/0.8                              | 23.72   | 22.58  | 0.41   | 0.75   | 0.39   | e      | 0.71   | 0.86 |              |                           |
|         | 2.3                   | -5.6                  | 6.1/1.1                              | 23.83   | 22.51  | -0.69  | 0.50   | 0.82   | e      | 0.51   | 0.62 |              |                           |
|         | -1.1                  | -6.4                  | 6.5/1.2                              | 23.67   | 22.08  | -0.24  | 0.39   | 1.20   | e      | 0.47   | 0.88 |              |                           |
|         | -8.5                  | 2.8                   | 9.0/1.7                              | 23.18   | 22.84  | -0.65  | 0.03   | 0.31   | e      | 0.39   | 0.28 |              |                           |
|         | 11.4                  | -6.3                  | 13.1/2.5                             | 23.56   | 22.48  | -0.78  | 0.37   | 0.71   | e      | 0.05   | 0.09 |              |                           |
|         | 0.2                   | -14.7                 | 14.7/2.8                             | >25.00  | 23.22  |        |        | > 1.08 | e      |        | 0.01 |              |                           |
|         | 0.0                   | 16.2                  | 16.2/3.0                             | 23.51   | 22.60  | -0.80  | 0.24   | 0.67   | e      | 0.01   | 0.01 |              |                           |
|         | -4.8                  | -17.6                 | 18.2/3.4                             | 23.10   | 21.46  | -0.34  | 0.77   | 0.87   | e      | 0.00   | 0.01 |              |                           |
|         | -6.3                  | 18.0                  | 19.0/3.6                             | 24.22   | >23.50 | -0.72  | 0.14   | < 0.58 | e      | 0.00   |      |              |                           |
|         | 17.3                  | 8.8                   | 19.4/3.6                             | 18.93   | <18.02 | -0.15  | 0.55   | > 0.36 | p      | 0.01   | 0.00 | 0.00         | G star                    |
|         | X306-42               | 3.1                   | -3.6                                 | 4.7/1.0 | 24.08  | >23.50 | -0.74  | 0.11   | < 0.47 | e      | 0.44 |              |                           |
| -3.6    |                       | 5.6                   | 6.6/1.5                              | 22.62   | 22.04  | -0.60  | 0.34   | 0.24   | p      | 3.18   | 1.23 | 1.065        | <b>AGN</b>                |
| -8.0    |                       | 2.1                   | 8.2/1.8                              | 24.03   | 23.29  | -0.25  | 0.02   | 0.72   | e      | 0.15   | 0.15 |              |                           |
| 10.4    |                       | -5.4                  | 11.7/2.6                             | 23.37   | 22.47  | -0.60  | 0.36   | 0.54   | e      | 0.08   | 0.09 |              |                           |
| -2.0    |                       | 12.2                  | 12.3/2.7                             | >25.00  | 23.40  |        | > 0.34 | 1.26   | p      |        | 0.02 |              |                           |
| 10.4    |                       | 11.8                  | 15.7/3.4                             | 22.03   | 21.19  | -0.10  | 0.54   | 0.30   | e      | 0.01   | 0.01 | 0.078        | NELG                      |
| X051-43 | 1.1                   | -1.1                  | 1.5/0.2                              | 21.44   | 20.60  | -0.12  | 0.48   | 0.36   | p      | 9.00   | 5.70 | ?.???        | <b>Bl Lac</b> (?)         |
|         | -6.3                  | 6.9                   | 9.4/1.4                              | 24.45   | 23.55  | >-0.95 | < 0.15 | > 0.75 | e      | 0.13   | 0.10 |              |                           |
|         | -9.7                  | 5.2                   | 11.0/1.7                             | 23.39   | >23.50 | -0.50  | -0.05  | <-0.06 | e      | 0.27   |      |              |                           |
|         | -0.6                  | 13.9                  | 13.9/2.1                             | 24.28   | 22.68  | >-0.78 | 0.78   | 0.82   | e      | 0.04   | 0.09 |              |                           |
|         | -13.1                 | 4.8                   | 14.0/2.1                             | 23.71   | 23.59  | >-0.21 | -0.41  | 0.53   | e      | 0.07   | 0.03 |              |                           |
|         | 3.8                   | -17.4                 | 17.8/2.7                             | 24.22   | >23.50 | >-0.72 | <-0.08 |        | e      | 0.01   |      |              |                           |
|         | -12.2                 | -14.5                 | 19.0/2.9                             | 20.23   | 19.20  | -0.13  | 0.60   | 0.43   | e      | 0.04   | 0.01 | 0.096        | Starburst                 |
|         | -11.7                 | 16.6                  | 20.3/3.1                             | 23.86   | 23.51  | >-0.36 | -0.30  | 0.65   | e      | 0.01   | 0.00 |              |                           |
|         | -6.1                  | 21.2                  | 22.0/3.3                             | 23.00   | 21.52  | > 0.50 | 0.81   | 0.67   | p      | 0.01   | 0.01 |              |                           |
| X407-44 | -3.3                  | -4.7                  | 5.7/0.8                              | 21.41*  | 20.65  | -0.94  | 0.19   | 0.57   | p      | 5.68   | 3.59 | 1.821        | <b>AGN</b> <sup>(1)</sup> |
|         | 14.1                  | 0.9                   | 14.2/2.0                             | >23.50* | 21.08  |        |        | > 1.42 | p      |        | 0.67 |              |                           |
|         | -18.2                 | -16.0                 | 24.2/3.3                             | 22.73*  | 20.99  | -0.92  | 0.93   | 0.81   | e      | 0.00   | 0.00 |              |                           |
| X233-45 | 4.9                   | -5.8                  | 7.6/1.1                              | 24.86   | 23.72  | -1.30  | < 0.56 | > 0.58 | e      | 0.09   | 0.11 |              |                           |
|         | -8.4                  | -2.5                  | 8.8/1.2                              | 24.83   | 23.33  | -1.29  | 0.71   | 0.79   | e      | 0.07   | 0.14 |              |                           |
|         | -4.0                  | -8.8                  | 9.6/1.3                              | 22.55   | 21.86  | -0.82  | 0.19   | 0.50   | e      | 0.29   | 0.48 | ?.???        | low S/N                   |
|         | -9.2                  | 5.9                   | 10.9/1.5                             | 24.69   | 21.76  | >-1.19 | 1.64   | 1.29   | e      | 0.06   | 0.37 |              |                           |
|         | -11.0                 | 3.2                   | 11.5/1.6                             | 24.86   | 23.10  | >-1.36 | 0.57   | 1.19   | e      | 0.04   | 0.08 |              |                           |
|         | -13.3                 | -1.8                  | 13.4/1.9                             | 22.51   | 21.70  | -0.66  | 0.25   | 0.56   | e      | 0.12   | 0.20 | 1.180        | <b>AGN</b>                |
|         | -12.0                 | -11.9                 | 16.9/2.4                             | 21.29   | 18.62  | 1.19   | 1.51   | 1.16   | e      | 0.49   | 0.21 |              |                           |
|         | -16.1                 | 10.4                  | 19.2/2.7                             | 24.49   | >23.50 | -0.49  | < 0.19 |        | e      | 0.01   |      |              |                           |
|         | 6.3                   | 20.7                  | 21.6/3.0                             | 22.41   | 21.12  | -0.54  | 0.58   | 0.71   | e      | 0.01   | 0.01 |              |                           |
|         | -17.6                 | -17.0                 | 24.5/3.4                             | 24.50   | 23.34  | -0.69  | < 0.20 | > 0.96 | e      | 0.00   | 0.00 |              |                           |
| X109-46 | -1.9                  | -0.2                  | 1.9/0.4                              | 23.56   | 22.59  | -0.52  | 0.42   | 0.55   | p      | 2.25   | 0.58 |              |                           |
|         | 2.6                   | 3.6                   | 4.4/0.9                              | 23.63   | 23.10  | -0.52  | 0.29   | 0.24   | e      | 0.80   | 0.44 |              |                           |
|         | -6.2                  | 5.1                   | 8.0/1.7                              | 21.70   | 20.56  | -0.54  | 0.75   | 0.39   | e      | 0.74   | 0.60 | 0.269        | Starburst(C)              |
|         | 2.5                   | 7.6                   | 8.0/1.7                              | 24.60   | 22.96  | >-1.10 | 1.04   | 0.60   | e      | 0.11   | 0.36 |              |                           |
|         | 2.1                   | -9.2                  | 9.4/2.0                              | 24.30   | 21.36  | >-0.80 | 1.44   | 1.50   | p      | 0.10   | 1.51 | 0.00         | M star (E)                |
|         | 4.0                   | -9.8                  | 10.6/2.2                             | 22.79   | 20.06  | > 0.71 | 1.57   | 1.16   | p      | 0.71   | 0.79 | 0.00         | M star (F)                |
|         | 7.5                   | 9.1                   | 11.8/2.5                             | 24.78   | >23.50 | >-1.28 | < 0.48 |        | e      | 0.02   |      |              |                           |
|         | 0.5                   | -12.7                 | 12.7/2.7                             | 24.75   | 23.44  | >-1.25 | 0.83   | 0.48   | e      | 0.01   | 0.02 |              |                           |
|         | -4.9                  | 14.7                  | 15.5/3.2                             | 22.78   | 21.83  | -0.83  | 0.25   | 0.70   | e      | 0.01   | 0.01 | 0.626        | NELG (I)                  |
| X213-47 | -8.5                  | -13.4                 | 15.8/2.9                             | 24.70   | >23.50 | >-1.20 | < 0.40 |        | e      | 0.00   |      |              |                           |
|         | -13.8                 | -13.8                 | 19.5/3.5                             | 24.51   | 23.54  | >-1.01 | 0.25   | 0.72   | e      | 0.00   | 0.00 |              |                           |

| ID.     | $\Delta\alpha$<br>[ $''$ ] | $\Delta\delta$<br>[ $''$ ] | $\Delta'' / \frac{\Delta}{\varepsilon_x}$ | $m_B$  | $m_R$  | U-B    | B-V    | V-R    | $LR_B$ | $LR_R$ | $z$  | object notes |                                     |
|---------|----------------------------|----------------------------|---|--------|--------|--------|--------|--------|--------|--------|------|--------------|-------------------------------------|
| X022-48 | -1.7                       | -1.3                       | 2.1/0.5                                   | 22.21  | 19.86  | 0.72   | 1.40   | 0.95   | e      | 3.25   | 3.36 | 0.32:        | <b>Interactive gal</b><br>companion |
|         | -1.6                       | -4.6                       | 4.9/1.1                                   | 23.31  | 22.06  | -0.20  | 0.74   | 0.51   | e      | 1.30   | 1.47 |              |                                     |
|         | 5.9                        | -6.0                       | 8.5/2.0                                   | 24.04  | >23.50 | >-0.54 | -0.03  | < 0.57 | e      | 0.12   |      |              |                                     |
|         | 8.9                        | -7.9                       | 11.9/2.7                                  | 22.33  | 21.00  | -0.38  | 0.66   | 0.67   | e      | 0.09   | 0.07 | 0.474        | NELG                                |
|         | -3.3                       | 11.5                       | 12.0/2.8                                  | 21.90  | 20.70  | -0.38  | 0.64   | 0.56   | e      | 0.08   | 0.07 | 0.389        | early+[OII]                         |
|         | -10.0                      | -9.6                       | 13.9/3.2                                  | 23.76  | 22.55  | -0.25  | 0.71   | 0.50   | e      | 0.01   | 0.01 |              |                                     |
|         | -15.4                      | -0.6                       | 15.4/3.5                                  | 24.51  | >23.50 | >-1.01 | < 0.21 |        | e      | 0.00   |      |              |                                     |
|         | -6.5                       | -14.9                      | 16.3/3.7                                  | 21.03  | 20.01  | 0.01   | 0.64   | 0.38   | p      | 0.02   | 0.01 | 0.00         | F/G star                            |
| X215-49 | 5.4                        | -7.4                       | 9.2/1.7                                   | 23.12  | 22.44  | -0.69  | 0.18   | 0.50   | e      | 0.37   | 0.42 |              |                                     |
|         | -0.1                       | -14.3                      | 14.3/2.7                                  | >25.00 | 23.32  |        |        | > 0.98 | e      |        | 0.01 |              |                                     |
|         | 3.7                        | 14.9                       | 15.4/2.9                                  | 22.58  | 22.19  | -0.78  | 0.19   | 0.20   | e      | 0.02   | 0.03 | 1.053        | strong[OII] gal (C)                 |
|         | -3.1                       | 16.4                       | 16.6/3.1                                  | 23.62  | 22.47  | -0.60  | 0.59   | 0.56   | e      | 0.01   | 0.01 |              |                                     |
|         | 17.6                       | 0.0                        | 17.6/3.3                                  | 24.35  | 22.93  | >-0.85 | 0.77   | 0.65   | e      | 0.00   | 0.00 |              |                                     |
| X264-50 | 0.4                        | 3.5                        | 3.5/0.7                                   | 24.44  | >23.50 | >-0.94 | < 0.14 |        | e      | 0.45   |      |              |                                     |
|         | -2.1                       | -7.2                       | 7.5/1.4                                   | 21.84  | 20.77  | -0.42  | 0.49   | 0.58   | e      | 0.89   | 0.73 | 0.568        | <b>Starburst</b>                    |
|         | 3.1                        | -9.1                       | 9.6/1.8                                   | 23.46  | 22.20  | > 0.04 | 0.66   | 0.60   | e      | 0.31   | 0.36 |              |                                     |
|         | -7.6                       | -7.5                       | 10.7/2.0                                  | 24.60  | >23.50 | >-1.10 | 0.10   | < 1.00 | e      | 0.05   |      |              |                                     |
|         | -9.9                       | -8.7                       | 13.2/2.5                                  | 23.24  | 22.96  | -0.41  | -0.03  | 0.31   | p      | 0.14   | 0.02 |              |                                     |
|         | 17.8                       | 2.1                        | 17.9/3.4                                  | 23.53  | 22.06  | -0.17  | 0.64   | 0.83   | e      | 0.00   | 0.01 |              |                                     |

extended in the R band) at  $z = 0.281$  and a B star. We consider the Sey 1 galaxy as the most likely identification.

**X404-23:** its large error box makes the identification difficult. The  $3\sigma$  error box contains 18 sources and all of them have low LR values. We took spectra for three objects, finding a NELG galaxy (object G) and a Sey 2 galaxy (object N) at different redshifts, while the third one (object J) is a faint ( $m_B = 23.74$ ) M star. None of them is a convincing identification. Visual inspection of the X-ray image suggests the presence of two different sources, at about  $40''$  from each other, which our detection algorithm has not been able to separate. This is also supported by the large positional error resulting from the maximum likelihood fit. Since the two sources appear to have approximately the same number of counts, it is likely that both of them are very close to or just below our X-ray detection threshold.

**X408-30:** the radio source coinciding with X408-30 and indicated with a cross in figure 4 is not associated to any optical object (see Gruppioni, Mignoli and Zamorani 1999). If the radio and X-ray sources are really associated, then the optical counterpart of the X-ray source is fainter than our optical limit. The brightest object in the field (object C), but well outside the 95% error box, is a NELG at  $z = 0.814$ .

**X207-31:** all the objects in the error box are extended. We took spectra for two galaxies, one ( $m_R = 22.43$ ) just outside the  $1\sigma$  error box and the second one ( $m_R = 19.65$ ) just outside the  $3\sigma$  error box. Both of them have  $z \sim 0.58$ ; the second galaxy, which is the brightest and reddest of all the surrounding galaxies appears to be a cD in a cluster. (Figure 4 shows the spectrum of this galaxy). Just below our maximum likelihood threshold for

X-ray detection, at about two arcmin from X207-31, there is an other X-ray source in a position where an overdensity of faint galaxies is clearly seen. Three of these galaxies have the same redshift as those in X207-31. We therefore identify X207-31 with a cluster, probably interacting with a second cluster at a distance of about 1.5 Mpc.

**X250-34:** the error box contains only faint ( $m_B \geq 23.2$ ,  $m_R \geq 22.9$ ) extended objects, none of which with a large LR. No spectrum was taken for any object.

**X011-35:** the density of objects in the error box is twice as high as the average density in our catalog. We took spectra for the six brightest objects ( $m_R < 21.5$ ) finding three galaxies at  $z \sim 0.39$  (objects D, L and O in figure 4), one absorption line galaxy at  $z = 0.189$  (object A; this is the object closest to the X-ray position), one early-type galaxy at  $z = 0.586$  (object F). The redshift of this galaxy is about the same as that of the clusters discussed in connection with X207-31. The angular distance between X011-35 and X207-31 ( $\sim 5$  arcmin) corresponds to about 4 Mpc, suggesting the existence of a large scale structure at this redshift. The sixth spectrum (object I) has a very low S/N and no redshift was derived. The spectrum in figure 4 is the spectrum of the galaxy closest to the X-position among those at  $z \sim 0.39$  (D). On the basis of these results, although with some possible ambiguity, we identify the X-ray source with a group of galaxies.

**X234-41:** also in this error box the density of faint extended objects is twice as high as the average density. In particular, in the inner  $10''$  there are six extended objects with  $23 \leq m_B \leq 24$ , while about one would be expected. Although no spectrum was taken, because of the faintness of the objects, we tentatively identify this source with a group or cluster of galaxies. The bright object just outside

**Fig. 4.** Finding charts for the X-ray sources with 68% and 95% error boxes and spectra of the most likely identifications.

**Fig. 4.** continued

**Fig. 4.** continued

**Fig. 4.** continued



**Fig. 4.** continued

**Fig. 4.** continued

the  $3\sigma$  error box is a G star with a too large X-ray to optical ratio to be associated with the X-ray source.

**X233–45:** we took spectra of the two brightest objects ( $m_B \sim 22.5$ ) within  $15''$  from the X-ray position. Both of them are classified as extended. One spectrum is very blue, with low S/N and no redshift was determined; the second object is an AGN at  $z = 1.180$ , which we consider to be the identification. No spectrum is available for the more distant and brighter extended object, whose colours suggest a low redshift elliptical galaxy.

**X109–46:** the error box contains three relatively bright objects ( $m_R < 21.5$ ), two of which are point-like and one extended. The two stellar objects are two M stars (objects E and F in figure 4), while the extended one is a starburst galaxy at  $z = 0.269$  (object C). The two M stars appear to be too faint for being the counterpart of the X-ray source. The starburst galaxy might be considered a likely candidate. We note, however, that very close to the X-ray position, there are two faint, blue objects with LR values larger than that of the starburst galaxy. One of these two objects, classified as point-like, is a good candidate for being an AGN. Waiting for spectra for these objects, we consider this source not identified yet.

**X213–47:** no object appears in our optical catalogs within the 95% error box, although a very faint object ( $m_R \geq 24.0$ ) is barely detected in two different exposures of the R CCDs at  $\sim 2$  arcsec from the X-ray position.

**X022–48:** the noisy spectrum of the galaxy close to the center of the X-ray error box shows a narrow emission line which, if interpreted as [OII], corresponds to  $z = 0.32$ . Both the blue and the red CCDs show clear signs of interaction with a fainter, blue extended object located about  $3''$  south. Also on the basis of the LR values, we consider this complex of interacting galaxies as a likely identification. The two galaxies just outside the  $2\sigma$  error box have different redshifts, while the brighter, more distant point-like object is an F/G star.

**X215–49:** no obvious candidate is contained within the 95% error box. The spectrum of the galaxy just outside of it (object C) shows a strong [OII] emission line and MgII2800 absorption line at  $z = 1.053$ . Its LR is small and we do not consider this object as the correct identification.

**X264–50:** there is one object in the error box with LR  $\sim 1$ . It is a relatively bright ( $m_R = 20.77$ ) starburst galaxy at  $z = 0.568$ . Despite the presence of a much fainter ( $m_R \sim 23$ ) blue, point-like source which may be an AGN candidate, we consider the galaxy as a possible identification.

## 4. Discussion

### 4.1. Summary of identifications and not identified sources

On the basis of the criteria discussed above, we have found reliable spectroscopic identifications for 41 sources (82% of the total), indicated in bold face in the last column of

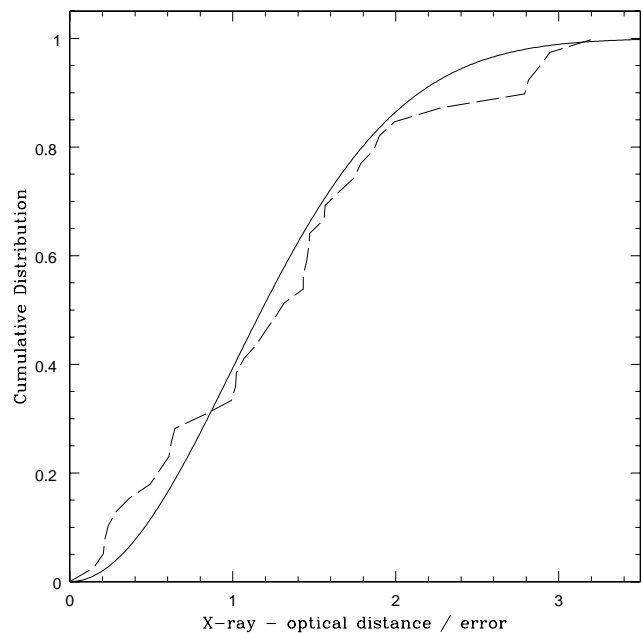


**Fig. 5.** Cumulative observed distribution (dashed curve) of the distances normalized to the error on each coordinate between the optical counterparts and the X-ray sources. Here we have excluded the three sources identified with groups or clusters of galaxies. The solid curve shows the expected distribution.

Table 3. For one more source (X234–41) the identification is very likely to be with a faint cluster of galaxy, although no redshift is available. These 42 reliable identifications are 33 AGNs (including the two radio galaxies and the BL Lac candidate; 79% of the identified sources), 2 galaxies, 3 groups or clusters of galaxies and 4 stars. Except for the higher fraction of unidentified sources (see discussion below), the identification content of this sample is in excellent agreement with what has been found, at a similar flux limit, in the much deeper PSPC and HRI surveys in the Lockman field (Hasinger et al. 1998, Schmidt et al. 1998).

Figure 5 shows the expected and observed cumulative distributions of the distances normalized to the error on each coordinate between the optical counterparts and the X-ray sources. In the observed distribution we have excluded the three sources identified with groups or clusters of galaxies, because for these objects it is more difficult to unambiguously define the optical position. The excellent agreement between the two distributions shows the goodness of our derived ML estimates for the positional uncertainties, at least when the X-ray position is not affected by confusion problems (see below).

If we divide our sample into two equally populated sub-samples as a function of flux ( $S > 6.5 \times 10^{-15}$  and  $S < 6.5 \times 10^{-15} \text{ erg cm}^{-2} \text{ s}^{-1}$ ), we find that the percentage of identifications remains approximately constant

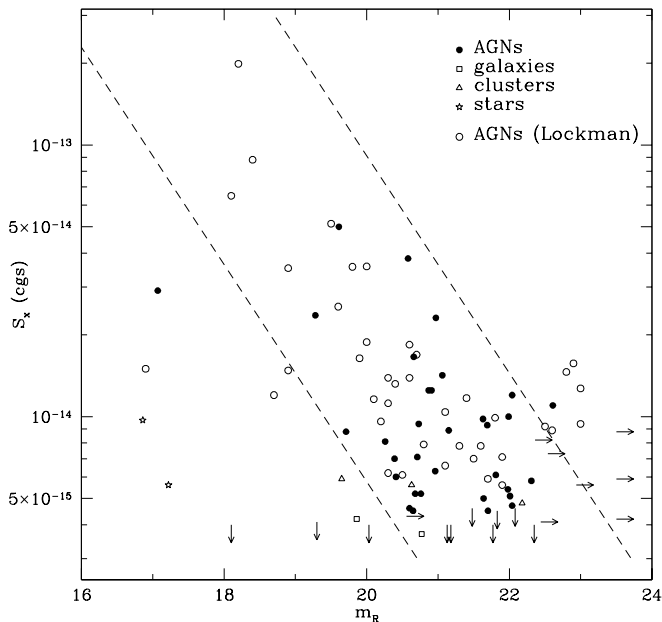


**Fig. 6.** X-ray flux versus  $m_R$  magnitudes for all the sources in our sample and for the AGNs identified in the Lockman Field (Schmidt et al. 1998). The two straight dashed lines, corresponding to constant X-ray to optical ratios, show the locus of this plane ( $-0.6 < \log f_x/f_v < 0.6$ ) which contains most of the identified AGNs in both samples. For a description of the upper limits, both in optical and in X-ray, see text.

(88% and 80% in the high and low flux sub-samples, respectively). AGNs are the dominant class of objects in both sub-samples (90% of the optical identifications in the high flux sub-sample and 65% in the low flux sub-sample), while the few identifications with clusters and galaxies are all in the low flux sub-sample. With the two extreme assumptions that none or all of the still unidentified objects are AGNs we derive that the percentage of AGNs among **all** the X-ray sources in our sample is comprised between 66% and 82%.

Figure 6 shows the X-ray flux versus  $m_R$  magnitudes for the sources in our sample and for the AGNs identified in the Lockman Field (Schmidt et al. 1998). The two bright F stars ( $m_B \sim 10$ ) are not shown here. The two straight dashed lines, corresponding to constant X-ray to optical ratios, show the approximate locus of this plane which contains most of the identified AGNs, both in our sample and in the Lockman Field. This range in X-ray to optical fluxes correspond to  $-0.6 < \log f_x/f_v < 0.6$ , where  $\log f_x/f_v$  is defined as in Maccacaro et al. (1988). For any given X-ray flux the range in magnitude is about  $\pm 1.5$ , corresponding to about  $\pm$  a factor of 4 with respect to the average X-ray to optical ratio. Despite the much higher X-ray flux limit and, correspondingly, much brighter limiting magnitudes, also most ( $\sim 90\%$ ) of the EMSS AGNs

lie in the same band. For the three sources identified with groups or clusters of galaxies we have plotted the magnitude of the brightest galaxies. The two X-ray sources identified with galaxies have an X-ray to optical ratio close to the lower limit of those of AGNs.

The limits for the eight unidentified sources are plotted at the magnitude of the brightest object within the 95% error box which is not excluded from being the optical counterpart on the basis of the available spectra. Three of these upper limits lie outside the band shown in the figure and three more are very close to the upper bound of this band. If associated with AGNs, they would have an X-ray to optical ratio significantly higher than the average. As shown in the figure, 6 such AGNs have been identified in the Lockman field; four of them are classical broad line objects, while the other two, showing only narrow lines, have been classified as AGNs on the basis of the presence of  $[\text{NeV}]\lambda 3426$  emission (Schmidt et al. 1998). The HRI arcsec positions in the Lockman field has made these identifications with such faint optical objects possible. In our case, with the 95% error radius for these sources ranging from  $8''$  to  $24''$ , similar identifications are significantly more difficult. Alternatively, we can not exclude that some of these sources may have a “wrong” position because of confusion. In Section 2 we have estimated that in about 2–5 cases a single source in our list may be produced by two different close-by sources, so that its position may be significantly wrong and we may not be able to find any reliable optical counterpart within the error box. The much more detailed simulations performed by Hasinger et al. (1998) show that in a PSPC survey like ours up to almost 20% of the detected sources with  $S_x < 1 \times 10^{-14} \text{ erg cm}^{-2} \text{ s}^{-1}$  (corresponding to about 7 sources) may appear at a detected position more than  $15''$  away from the true position because of confusion. From these considerations it follows that only higher resolution, deep X-ray data (e.g. with AXAF and XMM) can fully clarify the situation for these sources.

Some additional clues on the nature of the unidentified sources can be obtained from the analysis of the hardness ratio. Figure 7 shows the hardness ratio versus X-ray flux for the sources in the Marano field (panel a) and in the Lockman field (panel b).

Analysis of this figure shows the following results:

- i. Most of the sources in both fields occupy well defined bands in HR. On average, the observed hardness ratio values in the Lockman field are smaller than those in the Marano field. The reason for this shift in HR is essentially due to the lower  $N_H$  value in the Lockman field, so that the observed spectra appear softer. When converted to energy spectral indices, under the assumption of a single power law with the galactic  $N_H$ , the HR band in the Marano field corresponds to the range  $0.5 \leq \alpha_x \leq 2.0$ . Approximately the same range in  $\alpha$  is derived for the HR band in the Lockman field assuming  $N_H \sim 1 \times 10^{20}$ , i.e. approximately twice the value of atomic hydrogen de-

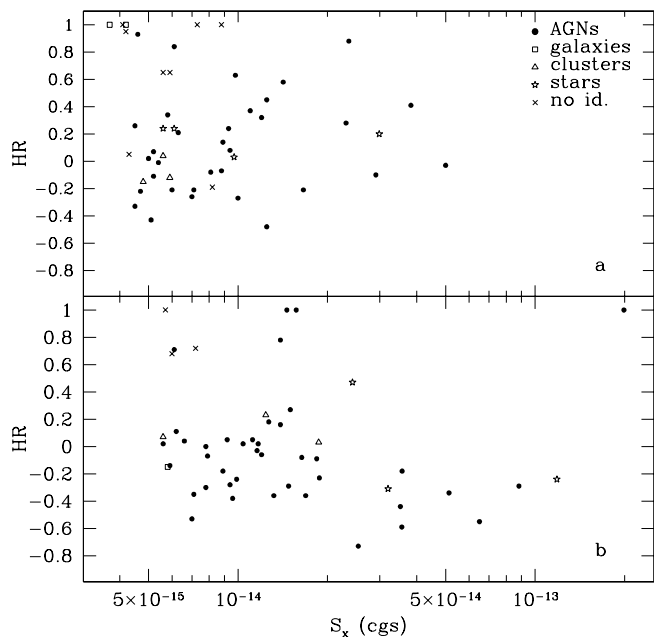


**Fig. 7.** Hardness ratio versus X-ray flux for the sources in the Marano field (panel a) and in the Lockman field (panel b). The symbols for the various classes of objects are shown in panel a.

rived from measurements in the 21 cm line (Lockman et al. 1986). A similar  $N_H$  value was derived by Hasinger et al. (1993) when fitting the average spectrum of all the X-ray sources in the Lockman field. This excess of X-ray absorption is consistent with the column density of ionized gas in the galactic disk derived from analyses of the dispersion measures of pulsars (Reynolds 1989). The presence of this additional column of ionised gas should be taken into account when analyzing ROSAT data, particularly in directions of low  $N_H$  as, for example, in the Lockman field.

ii. In both samples there are about (15–20)% of the sources which appear to have hard or absorbed spectra, with HR values close to 1. These sources appear to be reasonably well separated from the others, especially in the Lockman field where, because of the higher S/N ratio, the errors in HR are smaller. The fraction of sources without optical identification is significantly higher among these hard sources than among sources with “normal” X-ray spectrum. For example, in the Lockman field the unidentified sources are 3 out of 8 for sources with  $HR > 0.6$ , to be compared with zero out of 42 for sources with  $HR < 0.6$ ; in the Marano field the corresponding fractions of unidentified sources in the same HR ranges are 6/12 and 2/38. The eleven identifications (Lockman and Marano fields together) among these hard sources comprise 2 galaxies (X264–50 and X022–48), and 9 AGNs (4 broad line AGNs, 2 radio galaxies, 1 possible BL Lac, and 2 narrow line objects classified as AGNs on the basis of the presence of

[NeV] $\lambda$ 3426). This shows that AGNs are the dominant population also in this range of HR. However, contrary to what happens for objects with “normal” X-ray spectra, a relatively large fraction of them does not show the prominent broad lines typical of classical quasars. The absence of broad lines coupled with the presence of X-ray absorption are consistent with the standard unified models for AGNs. It is interesting to note that the two narrow line objects with [NeV] $\lambda$ 3426 have two of the highest X-ray to optical ratios in the Lockman field sample. Since the current optical limits for the unidentified sources in the Marano field correspond to X-ray to optical ratios similar to those of these sources, it is possible that at least some of our hard, unidentified sources belong to the same class of objects.

iii. In both samples, but especially in the Marano field, the hard sources tend to be more numerous at low flux levels. While this is likely to be, at least in part, a real effect, as shown by the identification content of these sources discussed above, there is also an obvious selection effect which favours hard spectra near the detection limit. At these fluxes, because of the combined effect of confusion and statistical fluctuations on small number of counts, a not-negligible fraction of the detected sources has measured fluxes significantly higher than the true fluxes (see Hasinger et al. 1998). Since the sample is defined in the ROSAT hard band, the measured hardness ratio for some of these sources would be biased toward large values and therefore the observed fraction of hard sources is probably higher than the real one.

#### 4.2. *Optically and X-ray selected AGNs*

As mentioned in Section 1, in the same area covered by the X-ray survey we have conducted in the past years a search for optically selected AGNs, using multi-colour data from plates taken at the ESO 3.6m telescope. (Zitelli et al. 1992). This survey has later been extended to fainter magnitudes using CCD data (Mignoli et al. in preparation) and has produced, so far, spectroscopic data for 29 optically selected broad-line AGNs inside the ROSAT area. Ten of these have not been detected in the X-ray data and their corresponding X-ray upper limits are shown in Figure 6. Three of these AGNs have X-ray upper limits outside the band shown in Figure 6, in the area of very low X-ray to optical ratio.

On the basis of the available CCD and spectroscopic data, which do not cover the entire ROSAT area of about 0.2 sq.deg., Mignoli and Zamorani (1998) estimate surface densities of  $\sim 185$  and 140 AGNs per sq.deg. with  $m_B < 22.5$  and  $22.5 < m_B < 23.5$ , respectively. These estimates are in good agreement with the predictions obtained by Zamorani (1995) on the basis of reasonable extrapolations from counts at slightly brighter magnitudes. Limiting ourselves at the classical broad-line AGNs and merging together the X-ray and the optically selected sam-

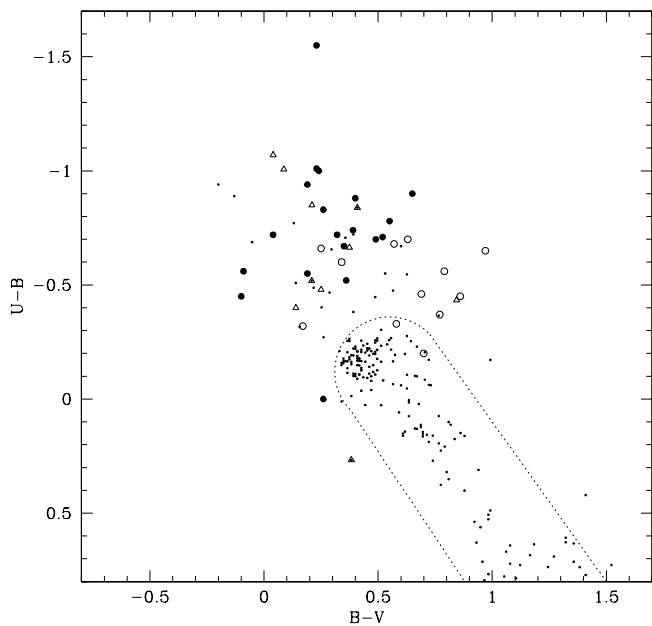


**Fig. 8.** U-B versus B-V for all the AGNs in our field. The different symbols represent AGNs detected in X-ray and already present in the optical sample (solid circles), AGNs detected in X-ray and not present in the optical sample (empty circles), AGNs not detected in X-ray (triangles). The small dots represent all the point-like objects in our CCD data with  $m_B \leq 22.5$ . The dotted curve shows the approximate locus occupied by stars in this plane.

ples, we have a total of 35 such objects with  $m_B \leq 22.6$  corresponding to a surface density of  $178 \pm 30$  broad-line AGNs per sq.deg. This is the highest reported surface density for these objects so far at this magnitude. Taking into account that, as mentioned above, the optically selected sample is not complete over the entire ROSAT area, this density is significantly higher than the estimate of about 125 AGNs per sq.deg. with  $m_B \leq 22.6$  recently obtained in the Deep Multicolor Survey, on the basis of 53 spectroscopically confirmed AGNs (Kennefick et al. 1997). Our estimated surface densities for  $m_B < 22.5$  and  $22.5 < m_B < 23.5$ , correspond to  $36 \pm 6$  and  $27 \pm 5$  AGNs inside the ROSAT area. Since in the same magnitude ranges ROSAT has detected 23 and 6 broad-line AGNs respectively, we conclude that the “efficiency” of AGN selection with X-ray exposures reaching about  $4 \times 10^{-15} \text{ erg cm}^{-2} \text{ s}^{-1}$  is  $\sim 65\%$  and  $\sim 20\%$  in the two magnitude ranges.

Having colours for all the X-ray selected AGNs, we can also estimate how many of them would have been missed by a purely optical selection. Figure 8 shows, with different symbols (see figure caption) all known AGNs in our field. The small dots represent all the point-like objects in our CCD data with  $m_B \leq 22.5$ . The dotted curve shows the

approximate locus occupied by stars in this plane. This figure shows that two X-ray selected AGNs (X251–37 at  $z = 2.71$  and X042–11 at  $z = 1.062$ ) are inside the star locus and therefore would have not been easily selected as AGN candidates on the basis of this diagram. Moreover, two X-ray selected AGNs (X233–45 at  $z = 1.180$ , and X409–28, the broad line radio galaxy at  $z = 0.958$ ) are classified as extended by our morphological algorithm and two more (X043–12, the AGN2 at  $z = 2.80$ , and X211–22 at  $z = 0.281$ ) have uncertain classification (i.e. p/e in Table 3). Since the colour-colour area occupied by faint AGNs contains a number of extended objects which is about ten times higher than that of the point-like ones, also these four objects would have not been easily selected as AGN candidates by purely optical data. Moreover, the location of these objects in the magnitude – redshift plane is not the same as that of AGNs which are more easily selected optically; five have  $m_B \geq 22.2$  and only one has  $m_B < 22.2$ , while the corresponding numbers for all the other AGNs with redshift in this field are 11 and 25. The same difference is also visible as a function of the absolute magnitude: five of the objects which would have been more difficult to detect from the optical data have  $M_B \geq -22.4$  and only one has  $M_B < -22.4$ , while the corresponding numbers for all the other AGNs are 14 and 22. This clearly shows that not only colour-colour selection of AGN candidates among point-like objects can be significantly incomplete at faint apparent magnitudes, but also the incompleteness increases at faint absolute magnitudes. As a consequence, if these not so stellar AGNs were really missed in faint optical surveys, this would introduce a bias in the derived optical luminosity function, which would appear flatter than the real one. Finally, we note also that a not negligible number of X-ray selected AGNs are significantly redder in B-V than the bulk of AGNs (see figure 8). Also this has to be taken into account in devising the most efficient optical selection criteria for faint AGN candidates.

## 5. Conclusion

We have presented the X-ray data and the optical identifications for a deep ROSAT PSPC observation in the Marano field. Careful statistical analysis of multi-colour CCD data in the error boxes of the 50 X-ray sources detected in the inner region of the ROSAT field (15' radius) has led to the identification of 42 sources, corresponding to 84% of the X-ray sample. These 42 reliable identifications are 33 AGNs (including two radio galaxies and one BL Lac candidate; 79% of the identified sources), 2 galaxies, 3 groups or clusters of galaxies and 4 stars. Except for the higher fraction of unidentified sources, the identification content of this sample is in excellent agreement with what has been found, at a similar flux limit, in the much deeper PSPC and HRI surveys in the Lockman field (Hasinger et al. 1998, Schmidt et al. 1998).

With simple simulations we have shown that in a few cases the reason for not having found an optical identification can be due to the fact that a single X-ray source in our list may be produced by two different close-by sources, so that its detected position may be significantly wrong. Most of the unidentified sources have a large ratio of X-ray to optical fluxes and harder than average X-ray spectra. Since most of the identified objects with these characteristics in our field and in the Lockman field are AGNs, we conclude that most of the sources with good position determination but without identification are likely to be AGNs.

Most of the sources in the Marano and Lockman fields occupy well defined bands in the plane hardness ratio versus X-ray flux. These bands correspond to the same energy spectral index range  $0.5 \leq \alpha_x \leq 2.0$ , only if the effective X-ray absorbing column in the Lockman field is about twice the value of atomic hydrogen derived from measurements in the 21 cm line. In both samples there are about (15–20)% of the sources which appear to have hard or absorbed spectra, with HR values close to 1 and, especially in the Marano field, they tend to be more numerous at low flux levels. However, since there is an obvious selection effect which favours hard spectra near the detection limit, it is difficult to quantify the reality of this effect. The fraction of sources without optical identification is significantly higher among these hard sources than among sources with “normal” X-ray spectrum. The eleven identifications (Lockman and Marano fields together) among these hard sources (9 AGNs and 2 galaxies) show that AGNs are the dominant population also in this range of HR. However, contrary to what happens for objects with “normal” X-ray spectrum, a relatively large fraction of them does not show the prominent broad lines typical of classical quasars.

Finally, comparing the optically and X-ray selected samples of AGNs in the same area, we estimate that the “efficiency” of AGN selection with X-ray exposures reaching about  $4 \times 10^{-15} \text{ erg cm}^{-2} \text{ s}^{-1}$  is  $\sim 65\%$  and  $\sim 20\%$  in the magnitude ranges  $m_B < 22.5$  and  $22.5 < m_B < 23.5$ , respectively. On the other hand, a not negligible fraction of the X-ray selected AGNs would have not been easily selected as AGN candidates on the basis of purely optical criteria, either because of colours similar to those of normal stars or because of morphological classification not consistent with point-like sources.

Moreover, the location of these objects in the magnitude – redshift plane is not the same as that of AGNs which are more easily selected optically. They tend to be fainter in terms of both apparent and absolute magnitudes. As a consequence, if these not so stellar AGNs were really missed in faint optical surveys, this would introduce a bias in the derived optical luminosity function, which would appear flatter than the real one. Finally, we note also that a not negligible number of X-ray selected AGNs are significantly redder in B-V than the bulk of

AGNs. Also this has to be taken into account in devising the most efficient optical selection criteria for faint AGN candidates.

*Acknowledgements.* The ROSAT project is supported by the Bunderministerium für Forschung und Technologie (BMFT), by the Science and Engineering Research Council (SERC) and by the National Aeronautics and Space Administration (NASA). This work was supported in part by NASA grants NAG5-1531 (M.S.), NAG8-794, NAG5-1649 and NAGW-2508 (R.B. and R.G.). G.H. acknowledges the DARA grant FKZ 50 OR 9403 5; G.Z. acknowledges partial support by the Italian Space Agency (ASI) under ASI contract ARS-96-70 and by the Italian Ministry for University and Research (MURST) under grant Cofin98-02-32.

## References

- Almaini O., Boyle B.J., Griffiths B.J., Shanks T., Stewart G.C., Georgantopoulos I., 1995, MNRAS, 277, L31  
 De Ruiter H.R., Zamorani G., Parma P. et al., 1996, A&A, 319, 7  
 Flynn C., Gould A., Bahcall J.H., 1996, ApJ, 466, L55  
 Georgantopoulos I., Stewart G.C., Shanks T., Boyle T.J., Griffiths R.E., 1996, MNRAS, 280, 276  
 Giacconi R., Gursky H., Paolini F.R., Rossi B.B., 1962, Phys. Rev. Lett., 9, 439  
 Gruppioni C., Zamorani G., De Ruiter H.R., Parma P., Mignoli M., Lari C., 1997, MNRAS, 286, 470  
 Gruppioni C., Mignoli M., Zamorani G., 1999, MNRAS, 304, 199  
 Hasinger G., Burg R., Giacconi R. et al., 1993, A&A, 275, 1 (erratum A&A, 291, 348)  
 Hasinger G., Boese G., Predehl P. et al., 1994, Legacy, 4, 40 (MPE/OGIP Calibration Memo CAL/ROS/93-015)  
 Hasinger G., Burg R., Giacconi R. et al., 1998, A&A, 329, 482 (Paper I)  
 Kenefick J.D., Osmer P.S., Hall P.B., Green R.F., 1997, AJ, 114, 2269  
 Lockman F.J., Jahoda K., McCammon D., 1986, ApJ, 302, 432  
 Maccacaro T., Gioia I.M., Wolter A., Zamorani G., Stocke J.T., 1988, ApJ, 326, 680  
 Marano B., Zamorani G., Zitelli V., 1988, MNRAS, 232, 111  
 McHardy I., Jones L.R., Merrifield M.R. et al., 1998, MNRAS, 295, 641  
 Mignoli M., 1997, Mem. S.A.It., Vol. 68, p. 335  
 Mignoli M., Zamorani G., 1998, in *The Young Universe*, D’Odorico S., Fontana A., Giallongo E (eds.), ASP Conference Series, Vol. 146, p. 80  
 Perlman E.S., Padovani P., Giommi P., Sambruna R., Jones L.R., Tzioumis A., Reynolds J., 1998, AJ, 115, 1253  
 Ratnatunga, K.U., Bahcall J.N., 1985, ApJS, 59, 63  
 Reynolds R.J., 1989, ApJ, 339, L29  
 Schmidt M., Hasinger G., Gunn J. et al., 1998, A&A, 329, 495 (Paper II)  
 Shanks T., Georgantopoulos I., Stewart G.C., Pounds, K.A., Boyle B.J., Griffiths R.E., 1991, Nature, 253, 315  
 Stocke J.T., Morris S.L., Gioia I., Maccacaro T., Schild R.E., Wolter A., 1991, ApJS, 76, 813  
 Sutherland W., Saunders W., 1992, MNRAS, 259, 413

- Zamorani G., 1995, in *Science with VLT*, Walsh J.R., Danziger I.J. (eds), ESO Ap. Symp, Springer, Berlin, p. 402
- Zitelli V., Mignoli M., Zamorani G., Marano B., Boyle B.J., 1992, MNRAS, 256, 349



This figure "rosat5\_fig1.jpg" is available in "jpg" format from:

<http://arxiv.org/ps/astro-ph/9904335v1>

This figure "rosat5\_fig4a.jpg" is available in "jpg" format from:

<http://arxiv.org/ps/astro-ph/9904335v1>

This figure "rosat5\_fig4b.jpg" is available in "jpg" format from:

<http://arxiv.org/ps/astro-ph/9904335v1>

This figure "rosat5\_fig4c.jpg" is available in "jpg" format from:

<http://arxiv.org/ps/astro-ph/9904335v1>

This figure "rosat5\_fig4d.jpg" is available in "jpg" format from:

<http://arxiv.org/ps/astro-ph/9904335v1>

This figure "rosat5\_fig4e.jpg" is available in "jpg" format from:

<http://arxiv.org/ps/astro-ph/9904335v1>

This figure "rosat5\_fig4f.jpg" is available in "jpg" format from:

<http://arxiv.org/ps/astro-ph/9904335v1>